# EXTENDING ELECTROCHEMICAL REPLICATION AND TRANSFER

**WANG HUIXIN**

**MPhil**

**The Hong Kong Polytechnic University**

**2021**

**The Hong Kong Polytechnic University**

**Institute of Textiles and Clothing**

# Extending Electrochemical Replication and Transfer

**WANG Huixin**

**A thesis submitted in partial fulfilment of the requirements for the degree of Master of Philosophy**

**December 2020**

# CERTIFICATE OF ORIGINALITY

I hereby declare that this thesis is my own work and that, to the best of my knowledge and belief, it reproduces no material previously published or written, nor material that has been accepted for the award of any other degree or diploma, except where due acknowledgement has been made in the text.

Wang Huixin

# Abstract

Patterning techniques are of great importance in various applications such as integrated circuits, display, micro-electromechanical systems, microfluid devices, and photonics. Extensive work has been done in developing patterning techniques, such as photolithography, electron beam lithography, nanoimprint lithography, scanning probe lithography, soft lithography, inkjet printing, screen printing, etc.

Recently, a new patterning technique called electrochemical replication and transfer (ERT) has been developed by our group which aims to achieve high resolution, high throughput and low cost at the same time. ERT process consists of two major steps. One step is the electrochemical replication of pattern on designed template. The other key step is the transfer of patterned materials from template onto target substrate. To assist the transfer, a layer of self-assembled 1H,1H,2H,2H-Perfluorodecanthiol (PFDT) on gold is used as release layer to decrease the adhesion between electrodeposited layer and the template.

In this thesis, we employ a thin layer of chromic oxide to replace PFDT and demonstrate the applicability of ERT ($Cr_2O_3$) in obtaining various geometric patterns with different materials on various substrates. The application of ERT ($Cr_2O_3$) in the fabrication of stretchable conductor and micro-supercapacitor is also demonstrated. The mechanism of ERT ($Cr_2O_3$) process was analyzed.

In conclusion, ERT ($Cr_2O_3$) is explored in obtaining various geometric patterns with different materials on various substrates to extend the electrochemical replication and transfer technique. The mechanism of ERT ($Cr_2O_3$) process is analyzed from electrocrystallization and adhesion perspectives.

# Acknowledgements

First of all, I would like to thank Prof. Zheng Zijian for his constant support. I am very lucky to have Prof. Zheng as my supervisor. He is knowledgeable, kind and exerts positive effects on everyone surrounding him. His meticulous attitude towards research and ways of thinking inspire me a lot. He is a great leader who has a vision and brings out the best of his members. I have learned a lot from Prof. Zheng and I will apply what I have learned in the future to become a better person.

I want to thank Dr. Lu Xi for his constant help in research. He taught me the operation of instruments, the detailed ERT method and helped me for countless times. I would also like to thank all other members in Prof. Zheng's group for their help and accompany during my MPhil study, especially Prof. Ma Zhijun, Dr. Huang Qiyao, Dr. Hu Hong, Dr. Gao Yuan, Dr. Xiao Ting, Dr. Wang Wenshuo, Dr. Wang Lei, Dr. Zhang Yaokang, Dr. Ng Sze-wing, Dr. Chang Jian, Dr. Luo Yufeng, Dr. Li Peng, Dr. Liu Guoqiang, Dr. Wang Pengwei, Dr. Zhang Yuqi, Dr. Lin Zhiqiang, Dr. Li Dongdong, Dr. Chen Dongdong, Dr. Chen Lina, Dr. Gan Qi, Dr. Wu Zhongwei, Dr. Xu Junling, Mr. Xie Chuan, Mr. Shang Jian, Mr. Wang Shuaichen, Ms. Rong Mingming, Ms. Guo Qianyi, Ms. Zhuang Qiuna. I would also like to thank technicians and officers at The Hong Kong Polytechnic University, especially Ms. Lemona Kong, Mr. Patrick Pang, Ms. Rise Choi at Institute of Textiles and Clothing, Dr. Terrence Wong, Ms. Joyce Ho at Cleanroom, Dr. Hardy Lui at Material Research Center, for their patient guidance and help.

I want to thank my family for putting their trust in me and giving me the freedom to choose freely what I want to accomplish.

At last. I would like to thank the Internet, google engine, and some useful websites, such as ResearchGate, XiaoMuChong, etc. They are very helpful and changes the way to get information in research work and enables the discussion of ideas worldwide.

# Table of Contents

# List of Figures

# List of Abbreviations

| | |
|---|---|
| AFM | Atomic force microscopy |
| CV | Cyclic voltammetry |
| DI water | Deionized water |
| DMSO | Dimethyl sulfoxide |
| DNQ | DiazoNaphthoQuinone |
| DOF | Depth-of-focus |
| EIS | Electrochemical impedance spectroscopy |
| ERT | Electrochemical replication and transfer |
| MSC | Micro-supercapacitor |
| NA | Numerical aperture |
| PDMS | Polydimethylsiloxane |
| PET | Polyethylene terephthalate |
| PFDT | 1H,1H,2H,2HPerfluorodecanthiol |
| PI | Polyimide |
| PMMA | Poly (methylmethacrylate) |
| PPy | Polypyrrole |
| PVA | Poly (vinyl alcohol) |
| RIE | Reactive ion etching |
| SAM | Self-assembled monolayer |
| SCE | Saturated calomel electrode |
| SEM | Scanning electron microscope |
| SPL | Scanning probe lithography |
| XPS | X-ray photoelectron spectroscopy |
| XRD | X-ray diffraction |

# Chapter 1: Introduction

## 1.1 Background

Patterning techniques are of great importance in a variety of applications, such as integrated circuits, photonics, microsensors, micro-electromechanical systems, and displays.[7] Various patterning techniques have been developed to meet different demands. For example, photolithography has been an important part in the fabrication of integrated circuit. Screen printing is extensively used in garments printing.

The general trends in the development of patterning technique are towards high resolution, high throughput, and low cost.[8-9] To meet these requirements, electrochemical replication and transfer (ERT) has been developed. This new patterning technique uses the selective electrodeposition of materials on template to replicate the patterns, then the patterns made of target materials are transferred to preferred substrates by adhesives. To promote the transfer process, the adhesion between template and plated materials is decreased by modifying 1H,1H,2H,2H-Perfluorodecanthiol (PFDT) on the template before electrodeposition. This patterning method is suitable for fabricating a wide variety of materials into arbitrary shapes on a variety of flexible substrates which is very promising in the application of a variety of fields. However, as a newly developed method, there are still a lot of space left to study. So, following the principles of ERT method, here we developed a new release layer ($Cr_2O_3$) and studied its applicability and mechanism. To distinguish with the previous ERT method which uses PFDT as release layer, we put the name of release layer after ERT (ERT (PFDT) and ERT ($Cr_2O_3$)).

## 1.2 Research objectives

This research aims in extending the newly developed patterning technique electrochemical replication and transfer. The research objectives of this research are listed as follows:

1. To develop a new release layer ($Cr_2O_3$) that can be used in ERT process

2. To investigate the applicability of ERT with this new release layer ($Cr_2O_3$)

3. To study the mechanism of ERT ($Cr_2O_3$) process

4. To compare the ERT (PFDT) with ERT ($Cr_2O_3$)

5. To demonstrate the application of ERT ($Cr_2O_3$)

## 1.3 Research originality

In this research, a new release layer $Cr_2O_3$ was studied to replace the previously used PFDT in patterning technique, electrochemical replication and transfer. The applicability of this ERT ($Cr_2O_3$) to various metals, various geometries and various substrates has been demonstrated. And the mechanism has been analyzed. It's application in fabrication of flexible micro-supercapacitor has also been demonstrated.

## 1.4 Outlines of the thesis

This thesis is organized as follows:

Chapter 1 briefly introduces the background of patterning techniques and then the objective and originality of this research.

Chapter 2 provides a brief introduction of the principles and development of general patterning techniques.

Chapter 3 gives the methodologies, including the materials, the instruments, fabrication processes and characterization techniques used in this study.

Chapter 4 demonstrates the fabrication process of ERT ($Cr_2O_3$) method and its

applicability to fabricate various flexible metal patterns into various shapes on variety of substrates.

Chapter 5 analyzes the mechanism of ERT($Cr_2O_3$) from the electrocrystallization and adhesion perspectives and studies the comparison between ERT (PFDT) and ERT ($Cr_2O_3$).

Chapter 6 demonstrates the applicability of ERT ($Cr_2O_3$) in fabrication of flexible interdigital micro-supercapacitor devices.

Chapter 7 concludes the results of this study and discusses the outlook of ERT patterning method.

# Chapter 2: Literature Review

## 2.1 General introduction of patterning techniques

Patterning technique plays key role in many applications such as the fabrication of integrated circuit board, sensors, display, micro-electromechanical systems, micro-optical components, etc.[10-13]

Commonly used and studied patterning techniques are photolithography, electron beam lithography, nanoimprint lithography, soft lithography, scanning probe lithography, and some printing techniques such as inkjet printing, screen printing, flexographic printing, and gravure printing.

Patterning techniques can be classified to generation of patterns or replication of patterns,[14-15] additive manufacturing or subtractive manufacturing from different perspectives.[16]

The operational and mechanistic principles of general patterning techniques would be introduced briefly. The development of some key patterning techniques would also be introduced.

## 2.2 Principles and development of general patterning techniques

### 2.2.1 Photolithography

Photolithography uses photons to create solubility changes in photon-sensitive film to generate patterns. There are generally two kinds of photo-sensitive resists, positive resists and negative resists. In the case of negative photoresist, the part of resist exposed to light would be polymerized or crosslinked and becomes insoluble in developer. In the case of positive resist, the part of resist under exposure would dissolve in developer

faster than unexposed area, leaving the part of resist covered by mask. The patterns of photoresist can be replicated with target materials with basically two routes, etching and lift-off. In the etching route, target materials are firstly deposited on the substrate followed by s standard photolithography process. The patterned resist would protect the material underneath resist during etching. In lift-off process, target materials are deposited or selectively grown on resist-patterned substrate. Materials deposited on photoresist patterns would be washed away together with photoresist during the removal of photoresist leaving the materials in a counter pattern.

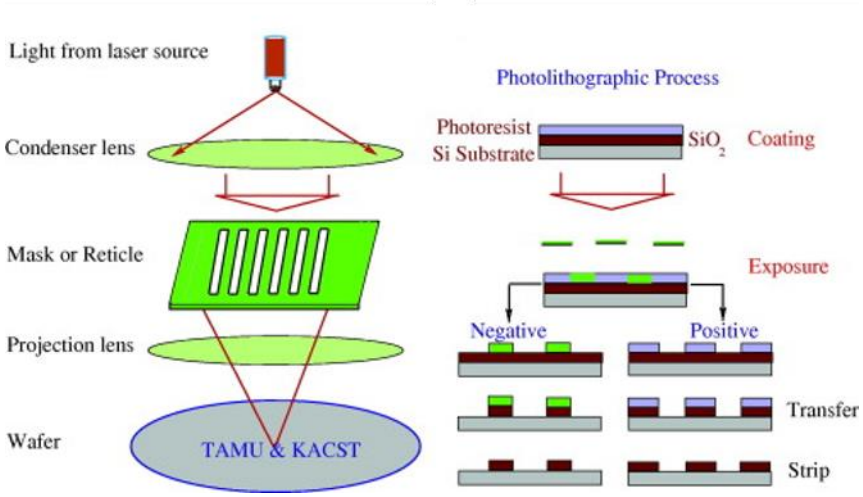


Figure 1. Scheme of mask-based photolithography and photolithographic process for positive resist and negative resist. [4]

The resolution of photolithography is limited by Rayleigh's equation.

$$R = k_1\lambda/NA$$

$$DOF = k_2\lambda/NA^2$$

Here, $k_1$ and $k_2$ are described as "process dependent constants", R is the minimum resolvable feature, λ is the wavelength of exposure light, NA is the numerical aperture, DOF is depth-of-focus.

According to Rayleigh equation, the minimum resolvable feature and depth of focus are limited by the wavelength of exposure light and the numerical aperture. DOF will become smaller inevitably with the improvement in resolution of feature. However, with a small DOF, the result patterns are more sensitive to the thickness of the photoresist layer which makes the process challenging.

Generally, changing exposure scheme, improving optical systems, reducing exposure wavelength and developing related resolution enhancement technologies are four main directions to improve the resolution of photolithography.[17-18] The exposure scheme has changed from early-stage contact printing scheme to projection scheme. In contact printing scheme, the resolution limit is around 2-3 μm. And the resist layer suffers from defects. So, projection exposure scheme was later used.[19] Increasing NA of lens is one approach to increase the resolution.[20] Since, high NA would cause drastically drop in DOF, further improvement of the resolution takes places in reducing the exposure wavelength. The exposure wavelength evolves from g-line (436 nm) to i-line (365 nm)[21], to KrF (248 nm),[22] to ArF (193 nm)[23], to $F_2$ (157 nm),[24] and to extreme ultraviolet (13.5 nm)[25]. To accommodate the change of exposure source, new lens materials, mask materials and resist materials should be developed, especially for extreme ultraviolet.[26] To overcome these difficulties in developing new materials, immersion system was proposed to reduce the effective exposure wavelength without changing the light source.[27] So, materials that are compatible for certain light source can be used to get patterns exceeding limited resolution without developing new materials. However, to meet the increasing demand of miniaturization, the use of shorter wavelength exposure source is inevitable. The resist materials compatible with shorter exposure wavelength source have been studied extensively.[28-29] Chemically amplifies resist was developed to provide better resolution for KrF and ArF exposure system.[30] Several resolution enhancement technologies have been proposed to elevate the resolution, such as phase shifting technology,[31] modified illumination,[32] optical proximity effect correction,[33] source and mask co-operation[34].

There are several challenges remaining for high-resolution photolithography, such as defects control, insufficient pattern fidelity when the resolution of patterns comes to

sub-10 nm. The drawbacks of photolithography are limited photoresists materials, waste of materials due to its nature of subtractive manufacturing, little control over functionality of surface, difficulty in fabrication of 3D structure.

### 2.2.2 Electron beam lithography

Electron beam lithography uses the energy of electrons to generate patterns in electron-sensitive resist. Electron has very small de-Broglie wavelength. Electron beam lithography can achieve high resolution to sub-10 nm easily.[35] Thus, electron beam lithography is less constraint in obtaining high resolution patterns. However, the writing time of electron beam is long with its limited beam current which can exceed 24 h per 1 $cm^2$.[36] The attempts to increase beam current would result in larger spot size due to the intrinsic repulsion of electrons and causes the loss of pattern fidelity.[37] The development of electron beam lithography is usually in the direction of increasing throughput instead of resolution. [16, 18] The commonly used resists in E-beam lithography process are methacrylic based positive resist such as PMMA and epoxy based negative resist such as SU-8.

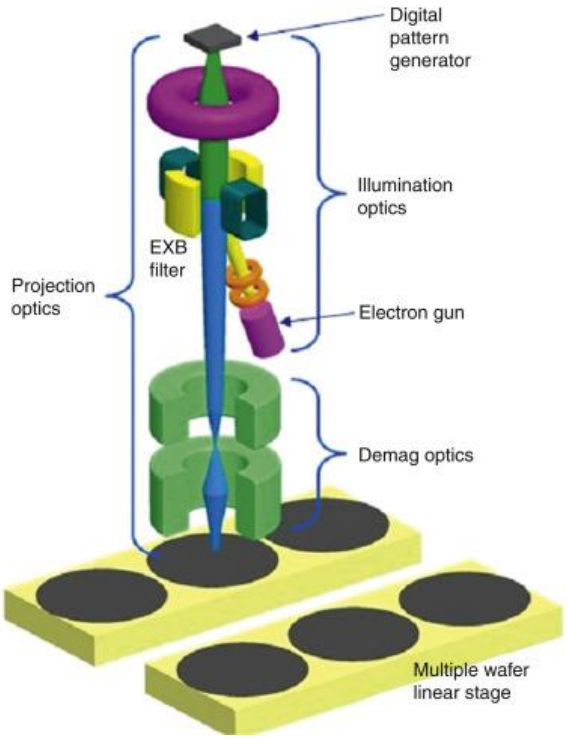


Figure 2. Schematic illustration of e-beam lithography.[3]

### 2.2.3 Nanoimprint lithography

Nanoimprint uses a hard mold to obtain mechanical deformation of resist material to form patterns.[38-39] By pressing the patterned mold on substrate covered by deformable resist, the height difference will be formed in resist under patterned region and non-patterned region of the mold. A thin layer of residual resist is left under the protrusion of mold to avoid direct contact of mold and substrate to protect the delicate nanoscale features. The thin layer of residual will be removed by reactive ion etching (RIE) or other techniques, leaving resist with higher height to form patterns. The fundamental principle of nanoimprint enables its resolution not to be limited by diffraction which is a common issue in photolithography. Nanoimprint is a high-resolution, high-throughput and low-cost technique. In the early stage of nanoimprint, the technique uses thermoplastic resists which needs to undergo a melting process to achieve phase change to facilitate mechanical deformation. The thermal mismatch between mold and substrate can cause pattern distortion. The patterns obtained by nanoimprint are more subjective to defects so the nanoimprint process cannot meet the stringent requirement of semiconductor fabrication.

Transparent mold and UV-curable liquid are developed to allow the nanoimprint process to be carried out at room temperature.[40]

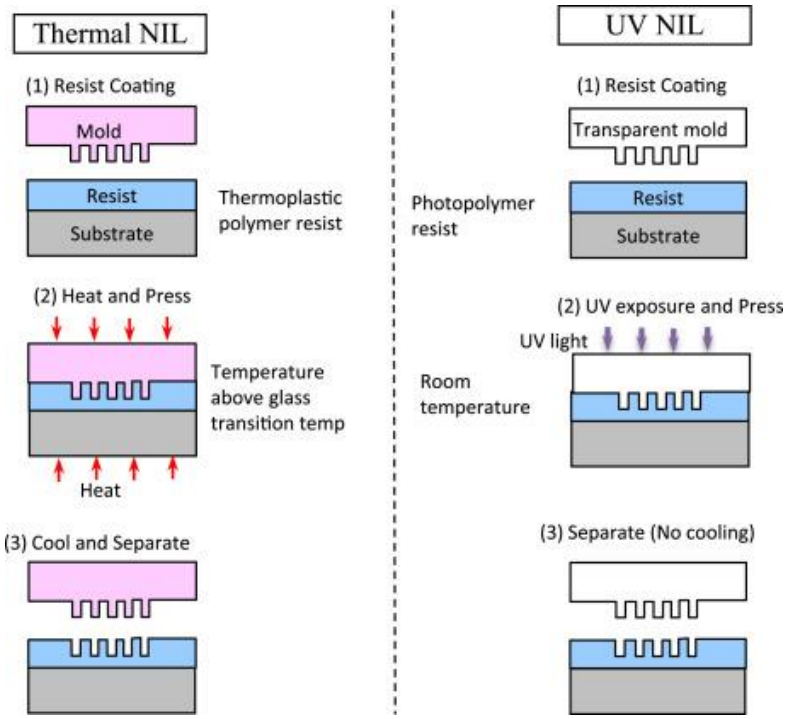


Figure 3. Schematic illustration of thermal nanoimprint lithography and UV nanoimprint lithography.[2]

### 2.2.4 Soft lithography

Soft lithography is a family of techniques for fabricating or replicating structures using elastomeric stamps, molds, and conformable photomasks. Microcontact printing (μCP), replica molding, microtransfer molding (μTM), micromolding in capillaries (MIMIC), solvent-assisted micromolding (SAMIM), phase-shift photolithography, cast-molding, embossing, and injection molding all belong to soft lithography.[6, 41-42] Microcontact printing is probably the most widely used method among soft lithography techniques.[43] Microcontact printing uses an elastomeric stamp with relief structure to print pattern of self-assembled monolayers (SAM) on the surface of substrates by contact.[42] The patterned SAM can protect the underlying substrates from certain wet etchants leading to selective wet etching.[42, 44] The patterned SAM can also be used to control the deposition of various materials such as metals, ceramics, conducting polymers, inorganic salts, and proteins to obtain corresponding patterned target materials. The most frequently used material for soft mold is polydimethylsiloxane (PDMS). PDMS has several advantages such as conformal contact with surfaces over relatively large areas, low interfacial free energy which makes it easily to be peeled off, good chemical stability, optical transparent which makes it applicable in patterning UV-curable materials.[45]

Challenges remain to be solved for soft lithography are the swell of PDMS in solvents,[46] the diffusion and disorder of SAM, limited aspect ratio of microstructures in PDMS due to its softness[42, 47], defects control in formed pattern, and difficulty in high-resolution registration.

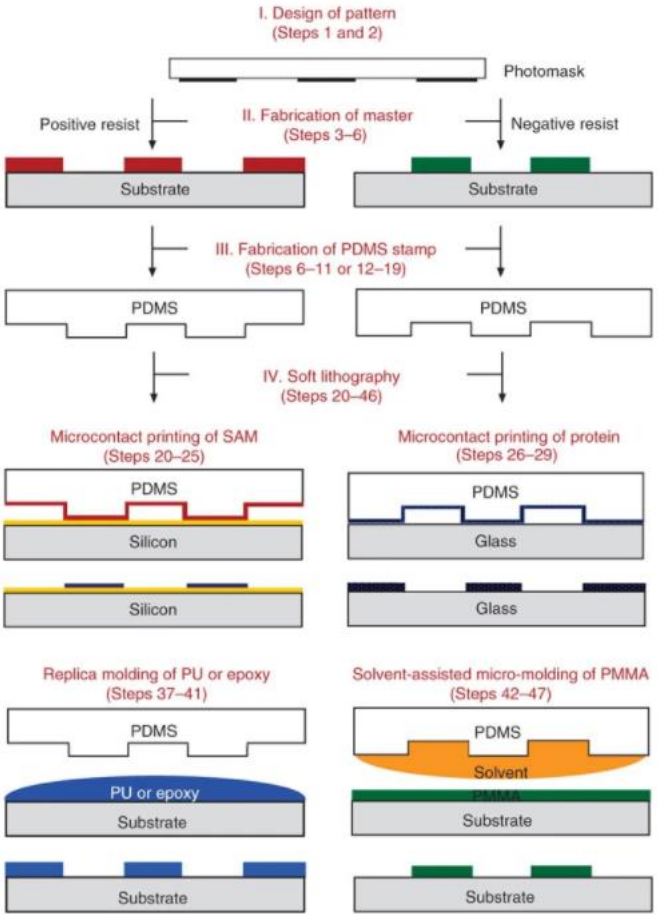


Figure 4. Schematic illustration of the four major steps involved in soft lithography and three major soft lithography techniques.[6]

### 2.2.5 Scanning probe lithography

Scanning probe lithography (SPL) can be used to selectively remove, react or transfer materials on substrate or to substrate respectively with a sharp probe.[48] SPL-based techniques can be classified as destructive or constructive methods. In destructive methods, the removal of part of the substrate is usually caused by mechanical abrasion using scanned AFM probe. In constructive methods, materials are delivered to the surface of substrate. The mechanism of the transfer of molecule form tip to substrate is complex and has intrigued many researchers. One hypothesis is the transfer of molecule from tip to substrate is assisted by the driving force caused by the interaction between ink and substrate induced by chemical interaction or other interactions.[49] The water layer between tip and surface might mediate material transfer by capillary force and gradient difference as well.[8] The feature size of patterns generated by SPL can go down to sub-10 nm easily.[50-52] However, this method is difficult to scale up. Although parallel writing has been proposed, it is still a relatively low-throughput patterning technique with its low writing speed.[53]

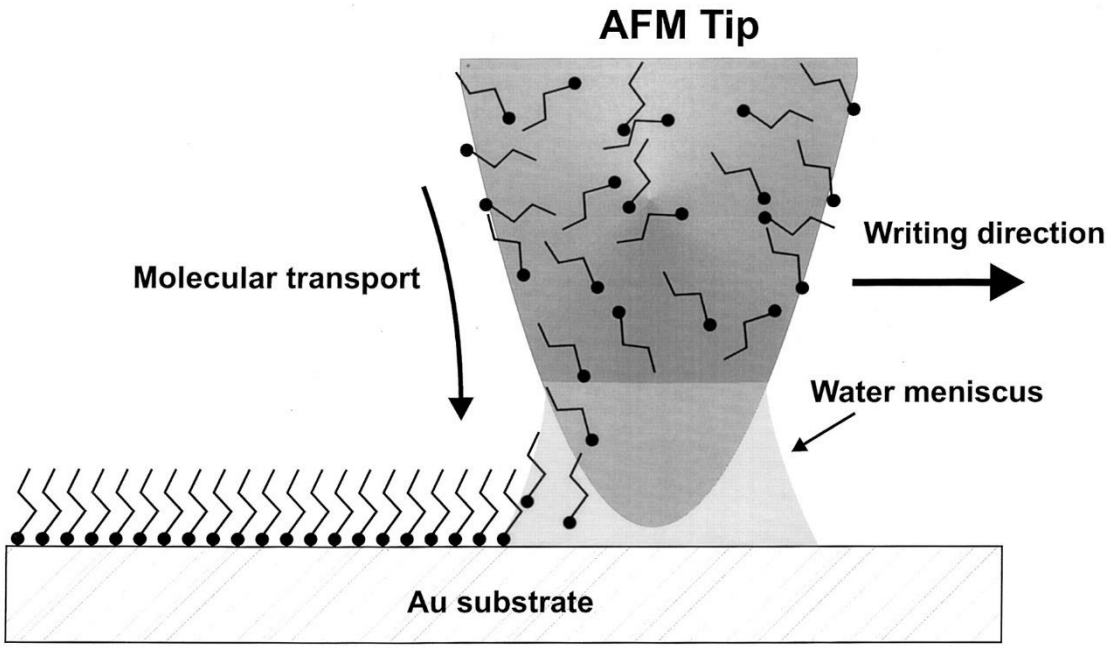


Figure 5. Schematic representation of dip-pen nanolithography.[1]

### 2.2.6 Printing techniques: inkjet, screen, flexographic, and gravure printings

Commonly used printing techniques are inkjet printing, screen printing, flexographic printing, and gravure printing.[5, 54]

Inkjet printing creates patterns by propelling droplets of ink onto substrate. There are two modes of inkjet printing: continuous and drop-on-demand.[55] The formation of droplet and the formation of inkjet-printed features on the substrate are two processes in inkjet printing that have been substantially studies by researchers.[5, 56-57] The fluid properties of ink and printing parameters affect deposition quality.[56] The ejection of droplet is completed usually with assist of piezoelectric printhead. The size of droplet propelled by inkjet printing usually limits its resolution.

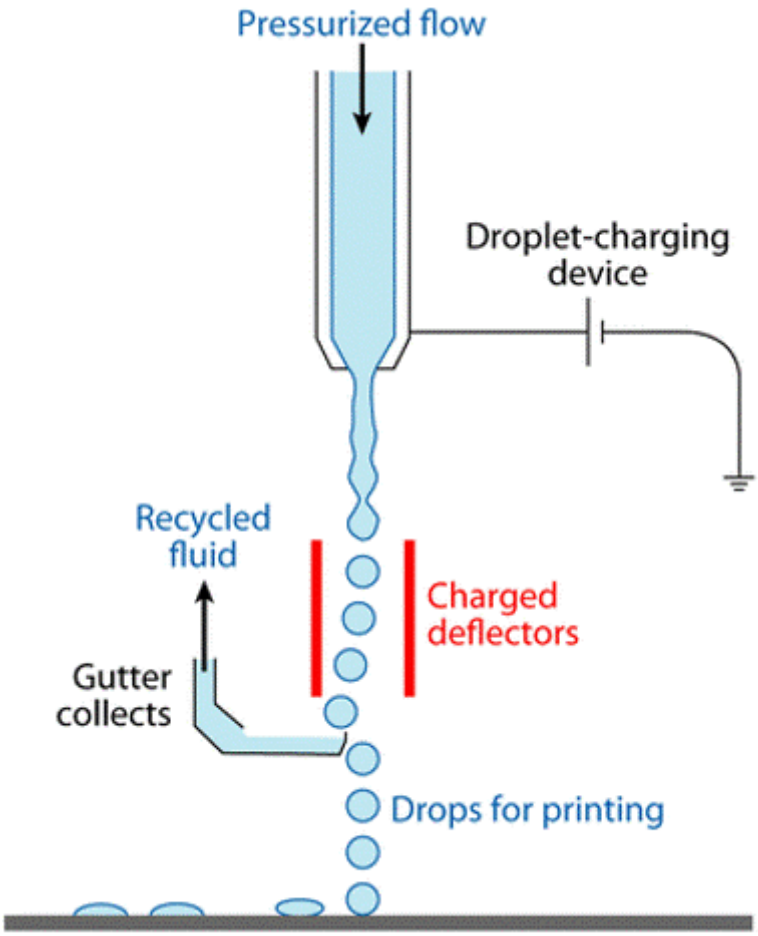


Figure 6. Schematic illustration of continuous inkjet printing.[5]

Screen printing, flexographic printing and gravure printing are conventional mass-printing techniques.[54] Screen printing uses a squeegee to press inks on substrate through a mesh screen. Screen printing is a simple and cost-effective process. The patterns obtained by screen printing are usually thick and the resolution of these patterns is limited (~50 μm). Flexographic printing uses a flexible relief plate to print inks on substrate. It is low-cost, applicable to wide range of materials and variety of substrates. However, the resolution of flexographic printing is limited (~100 μm). Gravure printing uses gravure roller with engraved pattern on surface to print inks. Gravure printing is of high throughput and applicable to wide range materials and substrates. However, the disadvantage of gravure printing, the same as the problem in screen printing and flexographic printing is the limitation in resolution (~50 μm).

# Chapter 3: Methodology

## 3.1 Materials

All the chemicals were used without further purification. Pure gold (Au, 99.999%, China New Metal), pure chromium (Cr, 99.999%, China New Metal), silicon wafer (Si, <100>, Suzhou Crystal Silicon Electronics and Technology Company, Ltd, China), silicon wafer with silicon oxide layer ($SiO_2$, <100>, 300 nm, Suzhou Crystal Silicon Electronics and Technology Company, Ltd, China), photoresist (AZ 5214E, Microchemicals GmbH, Germany), developer for AZ 5214E (AZ 300 MIF, Microchemicals GmbH, Germany), negative photoresist (NR9-1500PY, Futurrex, Inc., USA), developer for NR9-1500PY (RD6, Futturex, Inc., USA), Au etchant (Transene Company, Inc.), ethanol (ACS grade, Anaqua), isopropanol (ACS grade, Anaqua), acetone(ACS grade, Anaqua), 1H,1H,2H,2H-Perflurodecanethiol (PFDT, 97%, Sigma-Aldrich), dimethyl sulfoxide (DMSO, Unichem Laboratories Ltd.), commercial copper / gold / nickel plating solutions (Plug N Plate Cu solution, Plug N Plate Au Solution, Plug N Plate Ni Solution, Caswell Inc., USA), manganese (II) acetate tetrahydrate ($Mn(Ac)_2 \cdot 4H_2O$, 98% purify, Sigma-Aldrich), sodium sulfate anhydrous ($Na_2SO_4$, 99% purify, Sigma-Aldrich), lithium chloride (LiCl, 99%, Sigma-Aldrich), polyvinyl alcohol (PVA, Mw 89,000-8,000, 99+% hydrolyzed, Sigma-Aldrich), phosphoric acid, ($H_3PO_4$, 85w% solution in water, Acros Organics), Pyrrole (98%, Sigma-Aldrich), sulfuric acid ($H_2SO_4$, 95%, Sigma-Aldrich), hydrogen peroxide ($H_2O_2$, 30%, Sigma-Aldrich), NOA63 (Norland Optical Adhesive), SmartSolve dissolving tape (Amazon), polyimide (PI) tape, silicone elastomer 184 (SYLGARD), silicone elastomer curing agent (SYLGARD), commercial weighting paper, cotton cloth and nylon cloth, polyethylene terephthalate films (PET films, 125 μm, 50 μm, Suzhou Dawan Plastic Electronics Co. Ltd., China)

## 3.2 Fabrication of template

Photolithography and thin film deposition techniques are applied in the fabrication of template. For practical reasons, AZ 5214E and negative resist NR9-1500PY are both used in photolithography process. More than one mask aligner systems and thin film deposition techniques are utilized at different batches of the fabrication.

a) Photolithography process with AZ 5214E as image reversal resist

Si or $SiO_2$ wafer was spin-coated with AZ 5214E at 4000 rpm for 30 s. The wafer was then pre-baked on a hotplate at 100 ℃ for 90 s to remove the solvent. The wafer with solidified resist was exposed under a dose of 20 mJ $cm^{-2}$ UV light with self-designed photomask on it. After exposure, the resist was post-baked at 120 ℃ for 2 min on hotplate and then undergone a flood exposure with 300 mJ $cm^{-2}$ dose of UV light. Afterwards, the photoresist was developed in AZ 300 MIF developer for about 60-70 s. finally, it was washed with DI water and dried with compressed $N_2$. The wafer with patterned photoresist was then deposited with 5 nm Cr as adhesive layer, 40 nm Au and another 5 nm Cr as release layer. Finally, the sample was dipped in DMSO to remove the photoresist and get the patterned template.

b) Photolithography process with AZ 5214E as positive resist

Due to the design of photomask, positive resist was combined with etching method to get appropriate patterns. The Si or $SiO_2$ wafer was first deposited with a 5 nm thickness of Cr and 40 nm of Au layer. The sample was then spin coated with AZ 5214E at 4000 rpm for 30s. It was then baked on a hotplate at 100 ℃ for 90 s to remove the solvent. Then, the wafer with solidified resist covered by photomask was exposed under UV light with a dose of 40 mJ $cm^{-2}$. After exposure the photoresist was developed in AZ 300 MIF for about 60-70 s. The sample was washed with DI water and dried with compressed $N_2$. Au exposed on sample was etched away by dipping into a mixed solution of Au etchant and water with a ratio of 1:5 for around 2 min. After removing photoresist by DMSO, the sample was deposited with another layer of 5 nm Cr.

c) Photolithography process with NR9-1500PY

Si or $SiO_2$ wafer was spin coated with NR9-1500PY at 4000 rpm for 40 s. The wafer was then pre-baked on a hotplate at155 ℃ for 1 min to remove the solvent. The wafer with solidified resist was exposed under a dose of 175 mJ $cm^{-2}$ UV light with self-designed photomask on it. After exposure, the resist was post-baked at 105 ℃ for 3 min. Afterwards, the photoresist was developed with RD6 for about 10 s. Finally, it was washed with DI water and dried with compressed $N_2$. The wafer with patterned photoresist was then deposited with 5 nm Cr as adhesive layer, 40 nm Au and another 5 nm Cr as release layer. Finally, the sample was dipped in DMSO to remove the photoresist and get the patterned template.

AZ 5214E is a DNQ-Novolak photoresist. Novolak is a polymerized phenolic resin made of formaldehyde and phenol which is intended to protect the underlying substrate in subsequent processing. DiazoNaphthoQuinone (DNQ) in AZ 5214E is the photo-active substances that generate the differences in developing rates for exposed and unexposed area. The presence of DNQ in photoresist would reduce the developing rate in the unexposed area compared to photoresist that contains pure phenolic resin without DNQ. During exposure to UV light, the DNQ would be converted into carboxylic acid which largely increases the developing rate. So, the unexposed photoresist would be left on substrate to protect its underlying substrate from subsequent processing. To use AZ 5214E as image reversal resist, a baking step is needed after exposure to neutralize the carboxylic acid formed during exposure and activate the crosslinking agent in exposed area. A further flood exposure would generate carboxylic acid in previously unexposed area to increase the developing rate. Thus, image reversal process can be accomplished with AZ 5214E.

NR9-1500PY is a negative resist. The exposed area would be cross-linked in post-baking which reduces its developing rate in developer.

DMSO is used to remove the photoresist on wafer. Although the dissolving of resist in acetone is faster than that in DMSO, metal particles are easily left on the surfaces of templates during removing of resist from template made by lift-off method due to the volatility of acetone.

In the process of thin film deposition, thermal evaporation or e-beam evaporation is used to deposit thin metal film on pure wafer or resist-patterned wafer. The deposition rates of Cr and Au are around 0.1 Å/s and 0.5 Å/s respectively. The deposition rates are chosen to get uniform and robust templates. The wettability of Cr is good on $SiO_2$ wafer, so the deposition rate of Cr is controlled to a smaller rate to achieve better adhesion. In the case of Au, if the deposition rate is smaller than 0.2 Å/s, gold tends to form islands when the thickness of Au is around 20 nm. If the deposition rate of Au is larger than 1 Å/s, the adhesion between Au and Cr would be sacrificed. It should be noted that, the quality thin film is influenced both by parameters during deposition and the parameters of instrument for deposition, such as the size of chamber, the distance from source to substrate, etc. The prepared templates should meet the requirement for robustness and conductivity for subsequent ERT process.

Template without outer Cr layer was also fabricated for comparison.

## 3.3 Electrochemical replication and transfer with chromic oxide as release layer

The outer Cr layer would be naturally oxidized in ambient environment to form chromic oxide and serves as release layer in ERT process. The as-fabricate template (with chromic oxide as release layer) was immersed in copper/nickel/gold electroplating solution as working electrode with corresponding metal foils as counter electrode (Cu foil for Cu plating, Ni foil for Ni plating, and steel for Au plating). Due to the difference in conductivity between patterned area and non-patterned area, metals were selectively electroplated on patterned area of template. The electroplated metal layer was then peeled off with the assist of adhesives (NOA63 or dissolving tape). In the case of NOA63, NOA63 was dropped on the surface of electroplated template and cured by UV light with acceptor substrate (PET film, nylon fabric, PET fabric, weight paper, cellulose paper) placed on top of NOA63. The dose of UV light applied in curing was about 2500-5000 mJ $cm^{-2}$. After exposure, the electroplated metal patterns embedded in NOA63 was peeled off from as-fabricated ERT template. Dissolving tapes can be used to transfer metal patterns to substrates that are UV-opaque (PI film) or substrates that mismatch with NOA63 mechanically (PDMS).

## 3.4 Fabrication of micro-supercapacitor

Firstly, Au interdigital current collector was obtained by ERT ($Cr_2O_3$) process with NOA63 as adhesive and PET film as acceptor substrate. The current density and deposition time used in electroplating gold were 1.5 mA $cm^{-2}$ and 15 min respectively. Then, active materials ($MnO_x$, PPy) was electrodeposited on the current collectors to get $MnO_x$ or PPy symmetrical micro-supercapacitor, respectively. $MnO_x$ was electrodeposited on gold interdigital current collectors with 0.01 M $Mn(Ac)_2$ and 0.1 M $Na_2SO_4$ electrolyte under constant current density of 15 mA $cm^{-2}$ for various deposition times. Electropolymerization of pyrrole on gold interdigital current collectors was conducted with 0.15 M pyrrole and 0.1 M NaTps aqueous solution from -0.7 V to 0.8 V vs SCE at scan rate of 100 mV/s for 2 cycles. The electrochemical performance of electrodes was tested in 1 M $Na_2SO_4$ aqueous solution. For MSC device with $MnO_x$ as active material, the electrolyte was aqueous solution of 10 wt.% PVA and 20 wt.% LiCl. For MSC device with PPy as active material, the electrolyte was aqueous solution of 10 wt.% PVA and 10 wt.% $H_3PO_4$.

## 3.5 Characterization and techniques

### 3.5.1 Optical microscopy

An optical microscope uses visible light and a system of lenses to magnify images of samples. The optical microscope used here is Eclipse 80i, Nikon, Japan. The magnification of optical microscopic images ranges from 50x to 100x.

### 3.5.2 Atomic force microscopy (AFM)

AFM is a very-high-resolution type of scanning probe microscopy (SPM), which can provide nanometer-resolution images of samples in ambient (liquid) environments. It is applicable to characterize conductor, semiconductor, and non-conductors. AFM uses a cantilever with a sharp tip to measure the topography across a sample's surface. The force between the probe and the sample varies with the distance between atoms at the tip and atoms at the sample's surface. There are generally three operation modes for AFM imaging, contact mode, tapping mode, and non-contact mode. In contact mode, as a response to the changing of interatomic force, the cantilever bends or deflects thus changing the amount of light reflected to photodetector. Therefore, the surface topography of the sample can be translated from the data recorded by the photodetector. In non-contact mode, the tip of the cantilever does not contact the surface of the sample, which can prevent tip and sample from degradation. The distance between the tip and the sample is relatively large, the main interaction force between probe and sample in non-contact mode is the van der Waals force. Since the van der Waals force is very low in the non-contact regime, it is not possible to measure the deflection of the cantilever directly. Instead, it detects the changes in the phase or the vibration amplitude of the cantilever that are induced by the attractive force between the probe tip and the sample while the cantilever is mechanically oscillated near its resonant frequency. Tapping mode also uses the oscillation of cantilever to get feedbacks for surface topography which is similar to non-contact mode in principle of measurement.

Here, non-contact mode was used with XE-100 AFM from Park Systems in the

characterization of samples.

### 3.5.3 Scanning electron microscopy (SEM)

Scanning electron microscope acquires images of a sample by scanning the surface with a focused beam of electrons. The electrons interact with atoms in the sample, producing various signals (secondary electrons, back-scatter electrons, characteristic X-rays, transmitted electrons) that contain information about the surface topography and composition of the sample. The position of the beam is combined with the intensity of the detected signal to produce an image.

SEM TESCAN VEGA3 and SEM TM3000 Hitachi were used here. SEM TESCAN VEGA3 detects secondary electrons while SEM TM3000 Hitachi detects back-scattered electrons. Secondary electrons have low energies and short mean free path. So, secondary electrons can only escape from the very top surface of the samples. Back-scattered electrons are reflected from the sample by elastic scattering. They emerge from deeper part within the specimen. The intensity of back-scattered electrons signals is strongly related to atomic numbers of the composition for the specimen. So, back-scattered SEM can provide the element distribution in specimen.

### 3.5.4 Contact angle measurement

The wettability of a solid surface by a liquid can be studied with contact angle and Young-Dupre equation.

Here, SDC-350 (Dynetech, Inc., China) was used. 2 μL drop of deionized water was dropped on substrate controlled by SDC-350, then the image of water drop on surface of substrate was captured by CCD camera. The contact angle was calculated by software.

### 3.5.5 X-ray diffraction

X-ray diffractometer can analyze the structure of a crystal. The crystalline structure causes a beam of incident X-rays to diffract into many specific directions. By measuring the angles and intensities of these diffracted beams, the mean positions of the atoms in the crystal can be determined, as well as their chemical bonds, crystallographic disorder.

Here, X-ray diffraction patterns were collected on an X-ray diffractometer (Rigaku SmartLab 9 kW, Japan) with a Cu Kα X-ray source. The optics of XRD was aligned with medium resolution parallel beam configuration.

### 3.5.6 X-ray photoelectron spectroscopy (XPS)

X-ray photoelectron spectroscopy is a technique based on the photoelectric effect. XPS measures the kinetic energy and the number of electrons escaped from the sample into the vacuum of the instrument irradiated by a beam of X-rays. These data can be used to identify the elemental composition and its chemical state within the surface of the material.

Here, X-ray photoelectron spectroscopy data were collected on X-ray photoelectron spectrometer (ESCALAB 250, Thermo Scientific, USA).

### 3.5.7 Raman spectroscopy

Raman spectroscopy is a technique based on Raman scattering to identify the structures of molecules. Basically, a source of monochromatic light is used to interact with the sample through the molecular vibration, or other excitations which would cause the shift in the energy of photons and reveal the molecular vibration information of the sample.

Here, Raman spectra were collected using Raman microscope (Nomadic$^{TM}$ 3-in-1, BaySpec, USA). The samples were illuminated by a 532 nm laser with a 10× objective. Raman data were collected at room temperature with resolution of 1 $cm^{-1}$ and 30 s recording time.

### 3.5.8 Measurement of electrical resistance

Sheet resistance was obtained using a source meter (Keithley 2400 SourceMeter, Tektronix, Inc., USA) with four-probe method.

### 3.5.9 Stress-strain test

Stress-strain curves of PDMS were obtained with tensile strength tester (Instron 4411, Lab World Group, USA).

### 3.5.10 Electrochemical tests for micro-supercapacitors

Electrochemical workstation (CHI 660E, CH Instruments, Inc.) was used to test the electrochemical performance of micro-supercapacitor. The electrochemical performance of micro-supercapacitor under bending was obtained with the assist of a stepper motor linear stage (TSA50-C, Zolix, China).

# Chapter 4: Electrochemical replication and transfer with $Cr_2O_3$ as release layer (ERT ($Cr_2O_3$))

## 4.1 Introduction of ERT ($Cr_2O_3$)

ERT involves electrodeposition and transfer process. The fabrication procedure of template for ERT ($Cr_2O_3$) can be found in Chapter 3. The reusable template was made with photolithography and thin-film deposition technique. The fabrication process of ERT ($Cr_2O_3$) is schematically illustrated in Figure 7. A thin layer of Cr between Au and $Si/SiO_2$ serves as the adhesive layer to provide robustness of the template so that the template can be reused for multiple times. A thin layer of patterned Au would cause the difference in conductivity between Au-patterned area and region without Au on template. The difference in conductivity combining with suitable parameters in electrodeposition would lead to selective electrodeposition of target materials. The outer layer of Cr on template which was later naturally oxidized to $Cr_2O_3$ serves as a release layer to decrease the adhesion between electroplated layer and substrate and facilitate the transfer process. The electroplated patterns can be transferred to various substrates (PET film, nylon fabric, PET fabric, weight paper, PI film, PDMS film) by adhesives (NOA63, water soluble tape). Then, the template is reusable for next ERT process. ERT ($Cr_2O_3$) is fast and high-throughput method by employing electrochemical deposition to achieve the replication of pattern generated by relatively high-cost patterning technique such as photolithography. The major cost in ERT ($Cr_2O_3$) is the cost in the fabrication of patterned template which requests high-cost techniques such as photolithography and thermal evaporation. The reusability of ERT ($Cr_2O_3$) template would reduce the average cost for one ERT fabrication process.

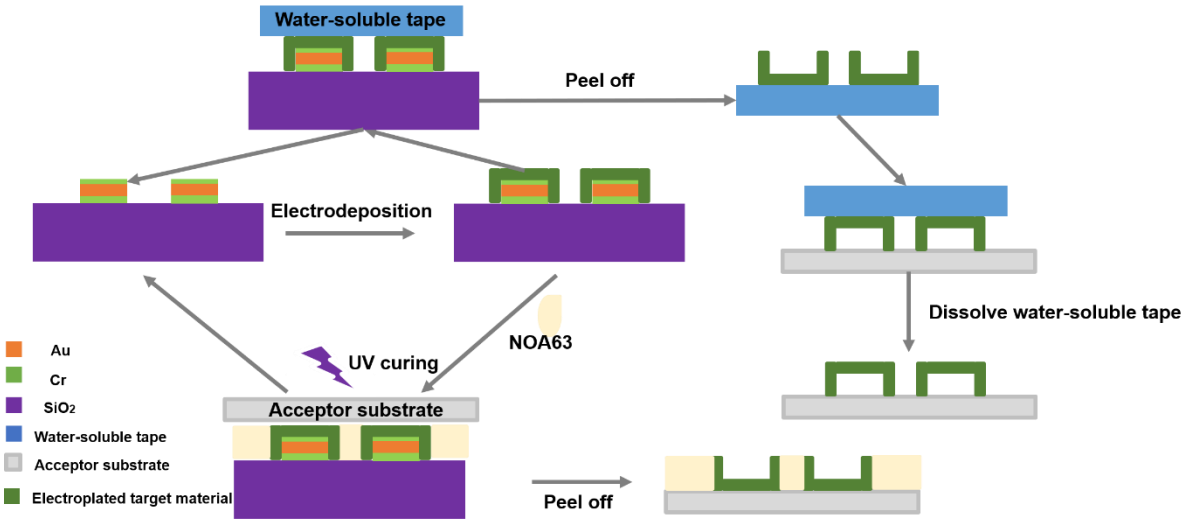


Figure 7. Schematic illustration of ERT ($Cr_2O_3$) process.

## 4.2 Fabrication of flexible metal patterns

With ERT ($Cr_2O_3$) process, we can obtain patterns of various metals with different geometries on various substrates.

As shown in Figure 8, flexible interconnected circuits can be achieved with ERT ($Cr_2O_3$) method. The circuit consists of straight lines, serpentine lines, circular and rectangular rings.

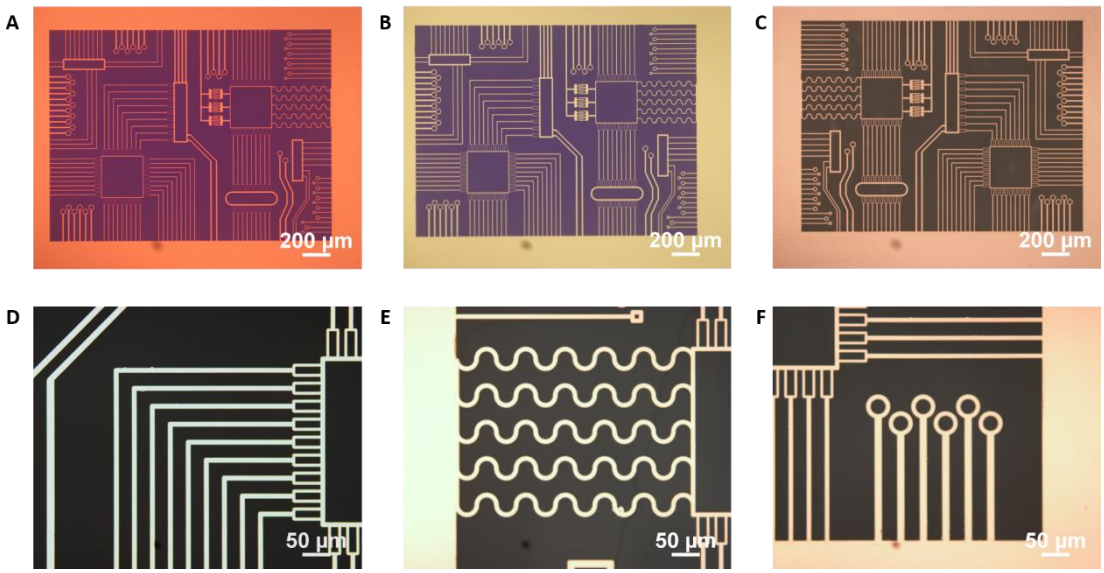


Figure 8. ERT method applicable to various geometric patterns. Optical images of (A) pristine template. (B) template after electroplating Cu. (C) Cu pattern transferred to PET film by NOA63. Zoom-in views of (D) straight lines (E) serpentine lines (F) circular and rectangular rings.

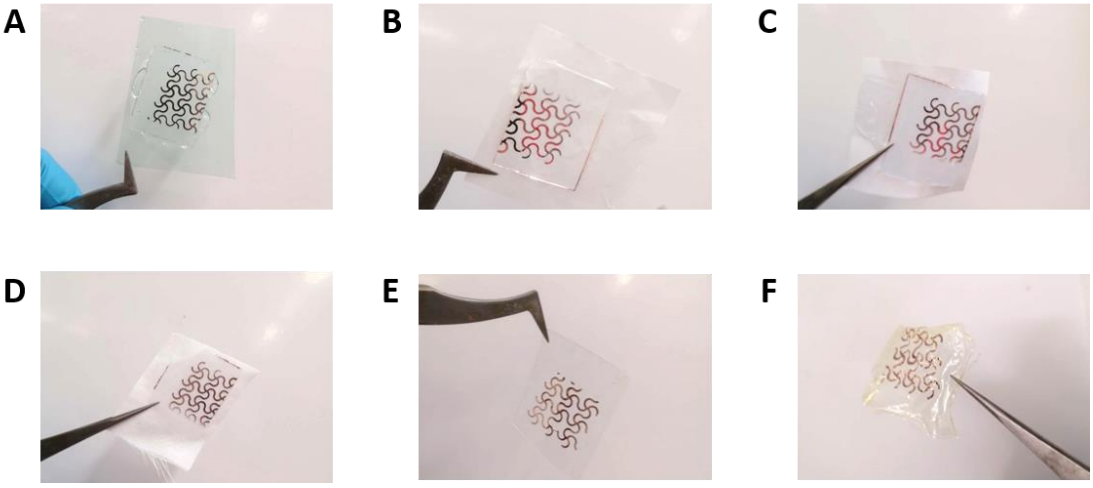


Figure 9. Copper patterns transferred to various substrate. (A) PET film, (B) weight paper, (C) cellulose paper, (D) fabrics, (E) PDMS, (F) PI film

Figure 9. shows the wide applicability of ERT ($Cr_2O_3$) to various substrates. Electroplated Cu serpentine interconnects can be transferred to PET film, weight paper, cellulose paper and nylon fabrics with NOA63 as adhesive. As Figure 7. shows, NOA63 was dropped on template after electrodeposition of Cu. Then, the acceptor substrate was covered on top of the NOA63. After UV curing, the Cu pattern can be peeled off from template to substrate with NOA63. The final metal patterns were embedded in the NOA63 which would provide better flexibility. However, NOA63 requires a UV-curing step which is not suitable for films that can absorb UV light efficiently such as PI film. Here, the PI film was made by spin coating a layer of precursor on $SiO_2$ wafer and followed by 30 min-heating at 100 ℃ on a hotplate. Water-soluble tape was used to peel off the Cu pattern from template. PI film and Cu was kept in closed contact for 1 h to bond with each other. Then, water-soluble tape can be dissolved, leaving the Cu on PI film. In the case of PDMS as the acceptor substrate, since NOA63 has a 6% elongation at failure which would mismatch with the stretchability of PDMS, it is preferred to get rid of the NOA63 layer. Thus, water-soluble tape was used to substitute NOA63 as adhesive to peel off Cu pattern from template. Then, Cu/water-soluble tape and $O_2$ pre-treated PDMS were kept in close contact for 30 min to enable enough bonding between Cu and PDMS. Finally, water-soluble tape was dissolved by drops of water, leaving Cu on PDMS.

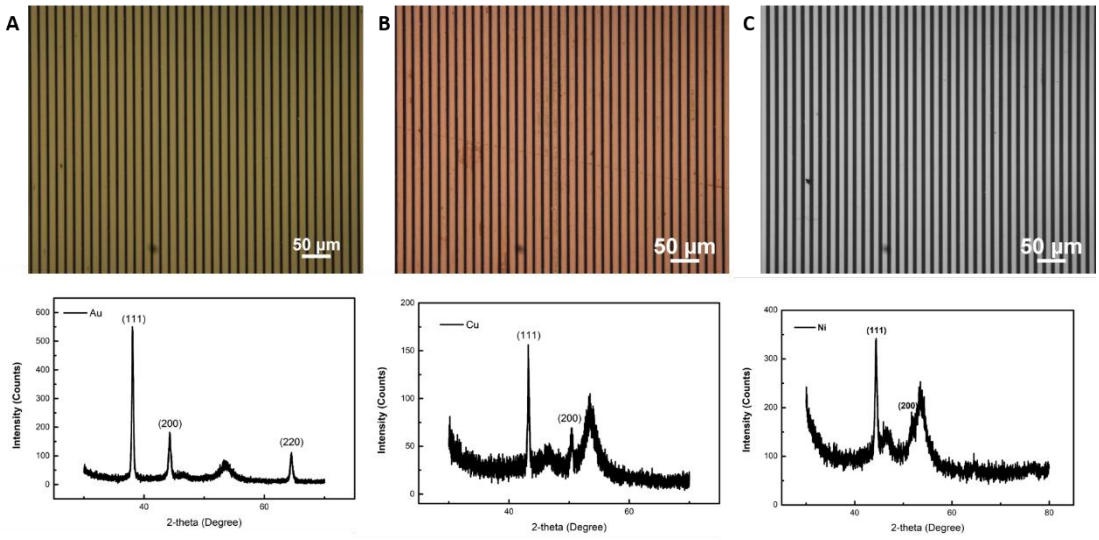


Figure 10. Various metal patterns made by ERT process. (A) Au and its XRD (B) Cu and its XRD (C) Ni and its XRD

Figure 10. shows the ERT ($Cr_2O_3$) method is applicable in obtaining Cu, Au, Ni patterns. For designed application, flexible patterns based on Cu, Au, Ni can be fabricated respectively.

The cyclability of template for ERT ($Cr_2O_3$) is demonstrated in Figure 11. The template can still serve after 30 cycles of ERT process. Cyclability is essential for decreasing the average cost of fabrication through ERT ($Cr_2O_3$). For template of ERT ($Cr_2O_3$), the inner Cr layer connects $SiO_2$ wafer and Au and increases the adhesion. The outer Cr layer adhered to Au is oxidized to $Cr_2O_3$ to decrease the adhesion between plated metal and template and thus protects the template in peeling process.

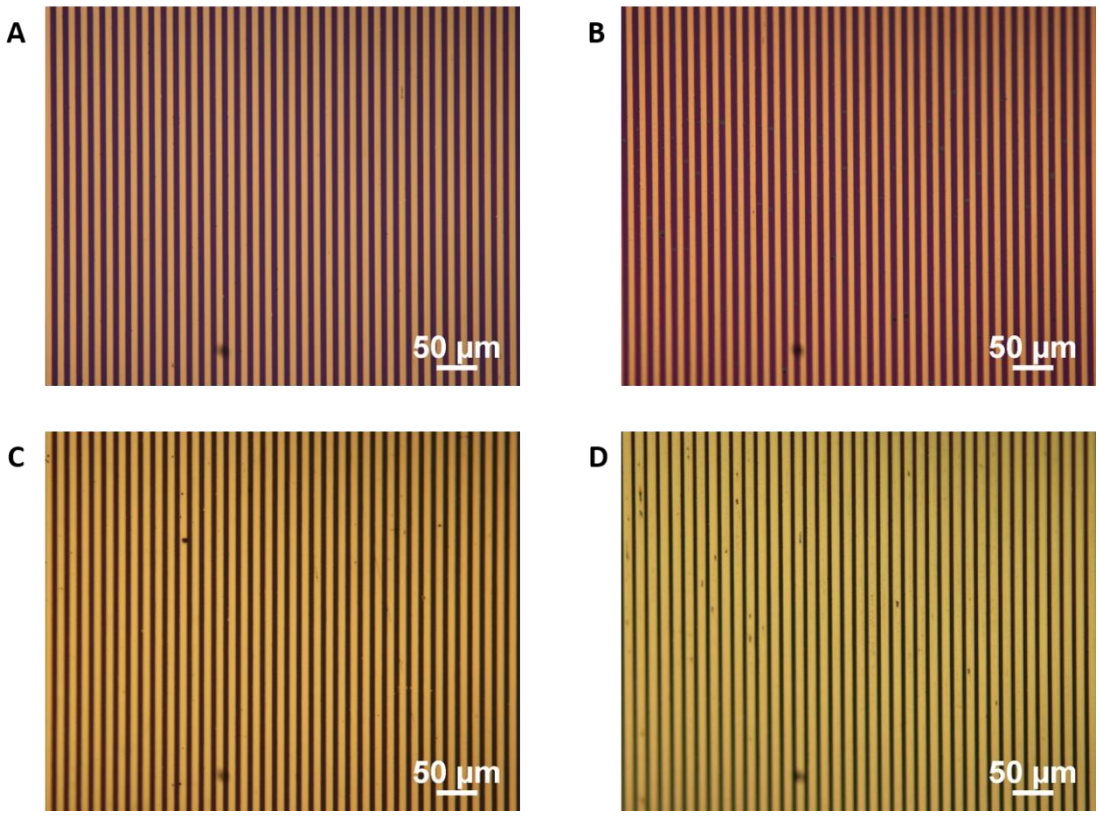


Figure 11. Cyclability of template. Optical images of (A) template after 15 cycles of ERT process, (B) template after 30 cycles of ERT process. (C) Au pattern on PET film obtained in the 15$^{th}$ cycle of ERT process, (D) Au pattern on PET film obtained in the 30$^{th}$ cycle of ERT process.

## 4.3 Fabrication of stretchable conductor

### 4.3.1 Introduction of stretchable conductor

Stretchable electronics can be applied in the field of robotic devices and wearable devices where traditional rigid electronics cannot fit in. Stretchable conductor as an indispensable part of stretchable electronics has been studied extensively by academics.

Stretchability and conductivity are two key parameters in the evaluation of stretchable conductor. Basically, there are three approaches to achieve both stretchability and conductivity in one material. The first approach is to design the structure of conductive yet non-stretchable materials to get stretchability. The second approach is to develop intrinsically stretchable and conductive materials. The third approach is to fabricate composites with both stretchability and conductivity by combining stretchable yet non-conductive materials with conductive yet non-stretchable materials.

Typical structures that can be stretched are serpentine structure, mesh, microcracks, wrinkle, wary structure, etc.[58] Typical materials that are both stretchable and conductive are liquid metal, conductive polymer, etc.[59] Stretchable conductor composites have also been developed. [60]

### 4.3.2 Preliminary results of stretchable conductors

PDMS substrate was prepared through standard procedure. The ratio between elastomer and curing agent was 10:1. The mixture was casted on PET film and cured in an oven at 80℃ for 2 h. Then the PDMS film was peeled off from PET film. The thickness of PDMS film used here was around 30 μm through SEM cross-section images (Figure 12A). The stress-strain curve of as-made PDMS thin film was recorded as in Figure 12B and 12C.

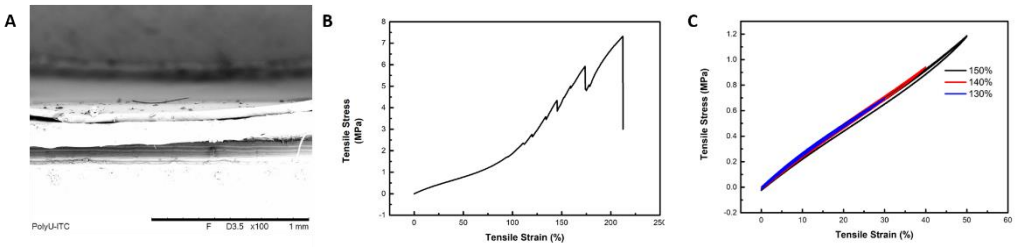


Figure 12. (A) Cross-section SEM images of PDMS. (B) (C) Stress-strain curve of PDMS.

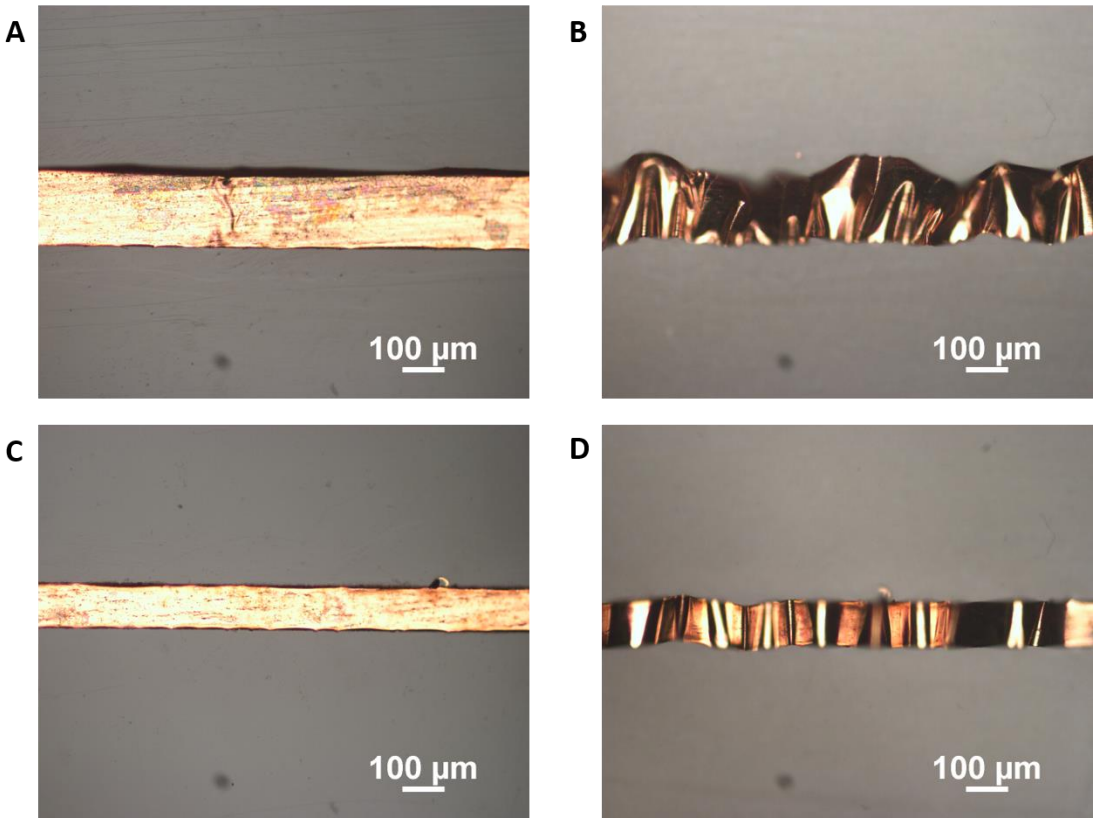


Figure 13. Digital images of (A) (C) copper straight line transferred to PDMS and (B) (D) copper line transferred to pre-stretched PDMS (30%) to form wary structure.

Cu straight lines and serpentine lines with different widths were obtained by electroplating at 3.5 mA cm-2 for 10 min. The Cu lines were transferred from template to PDMS with the assist of water-soluble tape (Figure 13, 14). By attaching Cu/water-

soluble tape to pre-stretched PDMS, wary structure can be formed after dissolving water-soluble tape and slowly releasing the strain in the pre-stretched PDMS. This wary structure would help improve the stretchability of Cu/PDMS composites. However, for Cu serpentine line, the strain tends to concentrate on the peaks and valleys thus the Cu film is easily broken during the release of pre-stretched PDMS (Figure 14).

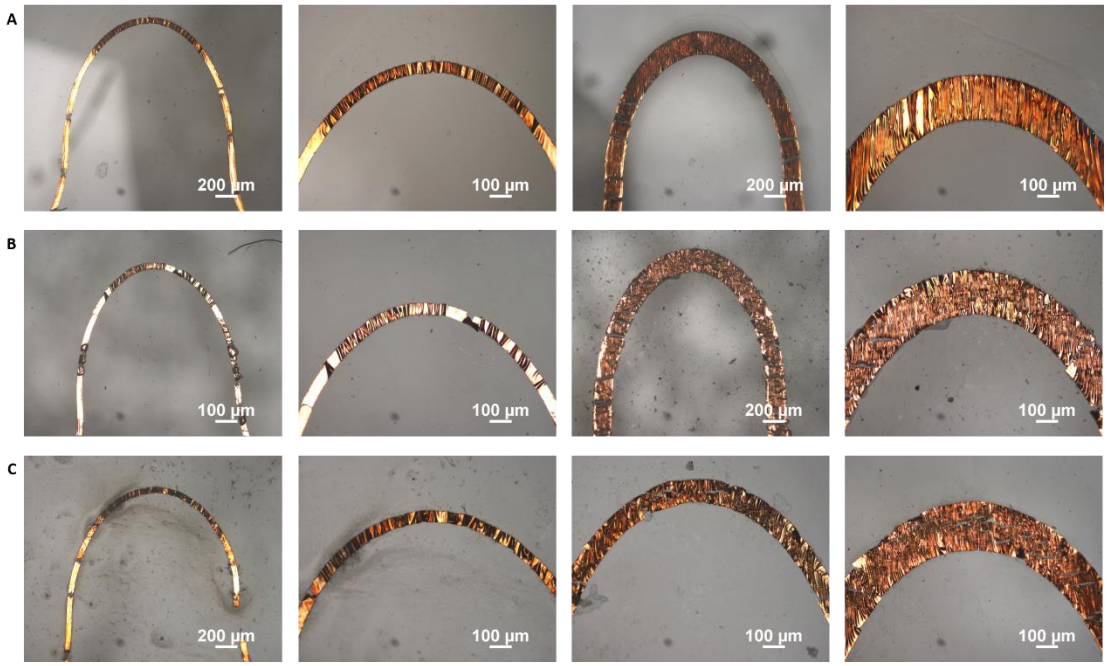


Figure 14. Copper serpentine line transferred to pre-stretched PDMS. The pre-stretch percentage is (A) 20% (B) 30% (C) 40% respectively.

The change in electrical resistance of Cu serpentine line attached to PDMS without pre-stretching under stretching was recorded (Figure 15.). The performance of this serpentine stretchable conductor has much space to be optimized.

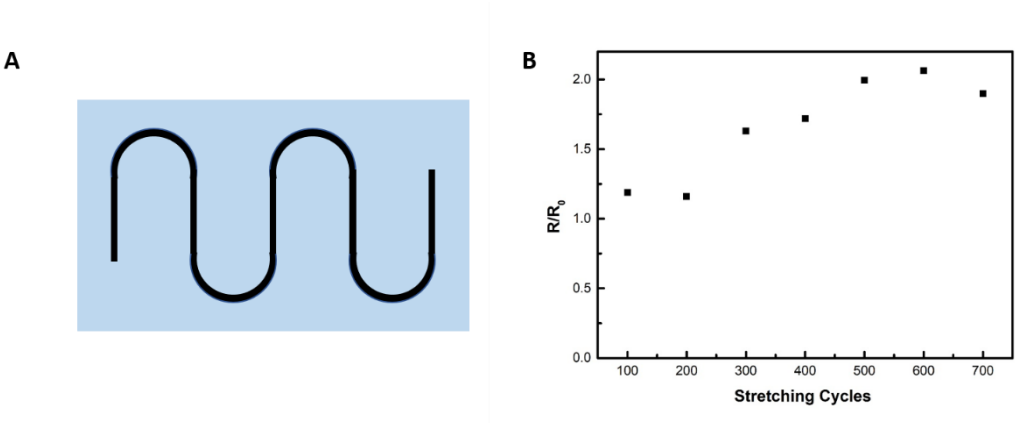


Figure 15. (A) Schematic of a copper serpentine line on PDMS film (The thickness of PDMS is around 30 μm). The length of arm and medium diameter of circle are 2200 μm. The width of the line is 200 μm. The thickness of Cu is around 2 μm. (B) $R/R_0$ versus stretching cycles for Cu serpentine line/PDMS.

## 4.4 Conclusion

Chromic oxide can be used as release layer for electrochemical replication and transfer. As demonstrated, this technique is suitable for fabrication of metal patterns with various geometries of micro-resolutions. The patterns can be transferred to various substrates by adhesives, such as flexible PET film, PI film, nylon fabric and stretchable PDMS. The resistivity change of the stretchable conductor made by ERT ($Cr_2O_3$) was tested under stretching.

# Chapter 5: Mechanism analysis of ERT ($Cr_2O_3$) process

## 5.1 Characterization of template

Schemes of several constructions of templates can be found in Figure 16. ERT contains two essential steps, electrodeposition and transfer. The difference in conductivity between substrate and Au-patterned area is essential for selective electrodeposition, i.e. the replication of patterns on template with electroactive materials. The Cr on template exposed in air would be oxidized into $Cr_2O_3$. A thin layer of $Cr_2O_3$ would change the conductivity of substrate by making the substrate made of Si wafer less conductive and the substrate made of $SiO_2$ more conductive. The structure of template would affect the parameters used in the electroplating process. The conductivity difference between substrate and patterns in B is the largest among these four structures which enables fast electroplating under high current density.

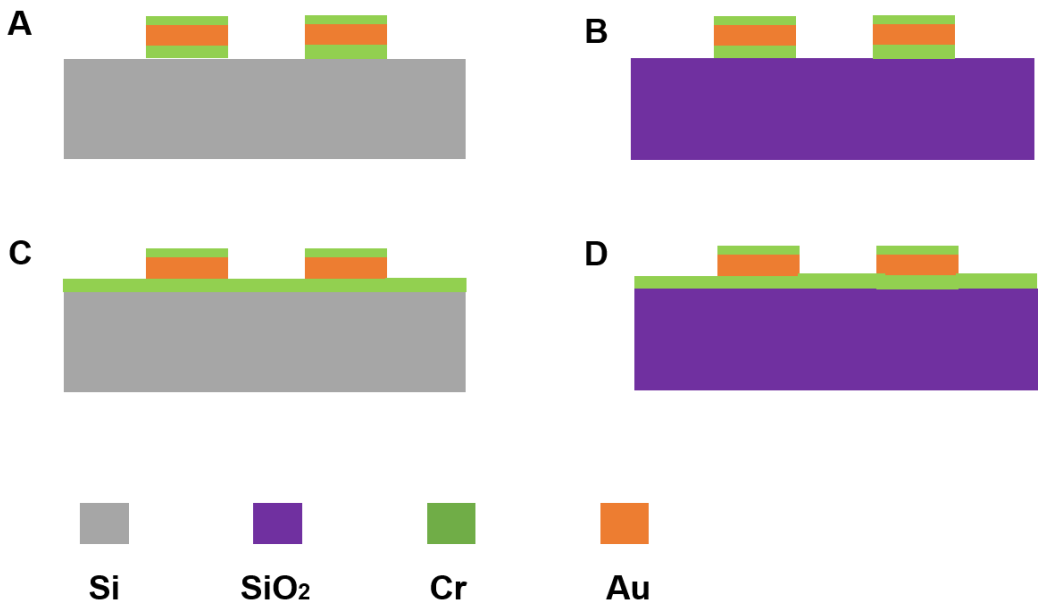


Figure 16. Scheme of templates.

The water contact angle shows that the surface of $Cr_2O_3$/Au/Cr/Si ERT template ($Cr_2O_3$) has high affinity to water. After the modification of PFDT, the water contact angle is slightly higher. However, the surface of template is still hydrophilic unlike the surface of Au/Cr/Si template after modification of PFDT. After the modification of trichloro(1H,1H,2H,2H-perfluorooctyl) silane, the surface became hydrophobic, which may indirectly prove the surface of template was naturally oxidized to chromic oxide. The location of Cr 2p peaks provide information on atomic valential state of Cr in the sample. For Au/Cr/Si template, no signal were detected for Cr 2p. this is because XPS is a highly sensitive surface analysis technology. It can penetrate a sample up to around 10 nm in depth.

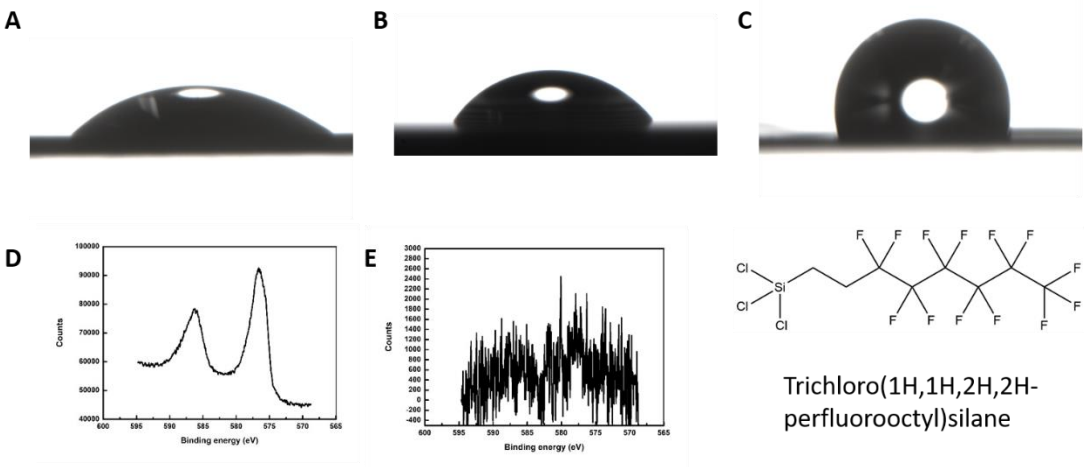


Figure 17. Water contact angle on (A) pristine template of ERT with $Cr_2O_3$ as release layer (B) template of ERT with $Cr_2O_3$ as release layer after PFDT modification (C) template of ERT with $Cr_2O_3$ as release layer after trichloro(1H,1H,2H,2H-perflurooctyl)silane modification (D) XPS for template of ERT with $Cr_2O_3$ as release layer ($Cr_2O_3$/Au/Cr/Si) (E) XPS for template of ERT with PFDT as release layer (Au/Cr/Si).

## 5.2 Role of $Cr_2O_3$ in ERT

Several mechanisms can lead to adhesion, for example mechanical interaction, diffusion, electrostatic force, covalent force, acid-base interaction, van der Waals force, etc. These mechanisms have different functional length scales and have different

energies.

The surface topography of template at nanoscale was obtained by AFM characterization. The roughness of the surface is related to the conditions during deposition of chromium such as evaporation speed. The physical contact area and the interactive forces between layers would affect the adhesion between these two layers. Here, we measured the surface morphology of electroplated Au which phase was in close contact to ERT ($Cr_2O_3$) template. From Figure 18B, the electroplated Au is not a conformable replication of the template in nanoscale. Instead, there are spaces between template and electroplated Au which would decrease the contact area and enlarge the average distance between electroplated Au and template, and thus lowers the adhesion between electroplated metal and template. The voltage profile during electroplating shows the difference in nucleation overpotential for both templates. The nucleation overpotential for ERT ($Cr_2O_3$) template is higher than that for ERT (PFDT) template which means the nucleation of Au on ERT ($Cr_2O_3$) is harder and the number of nucleation sites formed in initial stage would be smaller for ERT ($Cr_2O_3$) template compared with that on ERT (PFDT) template. This phenomenon is also confirmed by SEM images of Cu electroplating on both templates. On ERT (PFDT) template, the electroplated Cu has more sites to grow and the surface is smoother. On ERT ($Cr_2O_3$) template, the size of Cu particle is larger than that on ERT (PFDT) template. And, there are less Cu particles on the surface of ERT ($Cr_2O_3$) than ERT (PFDT), which means that Cu particles are tentative to cumulate on Cu instead of template in the case of ERT ($Cr_2O_3$), which may due to the ill conductivity of $Cr_2O_3$ and also the less infinity of Cu to $Cr_2O_3$.

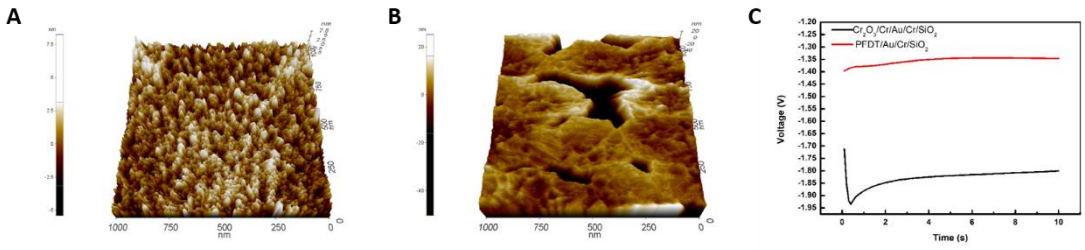


Figure 18. (A) Topography of template. (B) Topography of plated Au on the surface of template. (C) Voltage against time curves measured in electrodeposition of Au on PFDT/Au/Cr/$SiO_2$ and $Cr_2O_3$/Cr/Au/Cr/$SiO_2$ substrates under the same current density of 1 mA $cm^{-2}$.

The morphologies of Cu line after various deposition time (10 min, 15 min, 20 min, 25 min, 30 min) at 3 mA cm-2 were characterized by AFM. It shows that at initial deposition stage, the distribute of Cu along the line is not even. With longer deposition time, and the effect of electric field, the shape of Cu line is more likely to become higher at edges and more uniform in the middle. The rough surface of Cu provides more surface area to contact with adhesives and thus increases the adhesion between them and makes the transfer process easier.

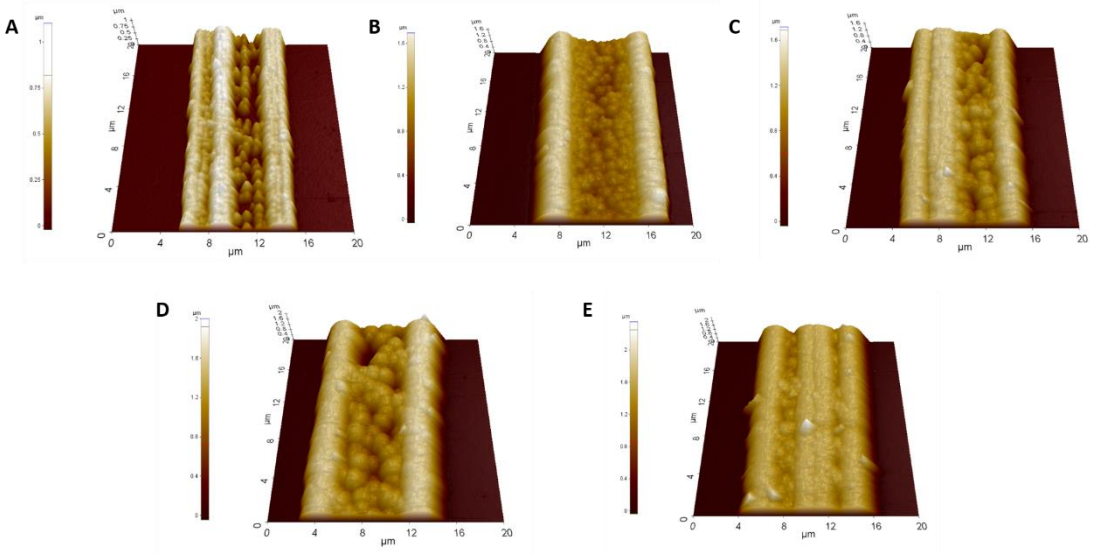


Figure 19. Topography of copper line on Cr/Au/Cr/$SiO_2$ template electroplated at 3 $mA/cm^2$ for (A) 10 min (B) 15 min (C) 20 min (D) 25 min (E) 30 min

## 5.3 Comparison of ERT ($Cr_2O_3$) method with ERT (PFDT) method

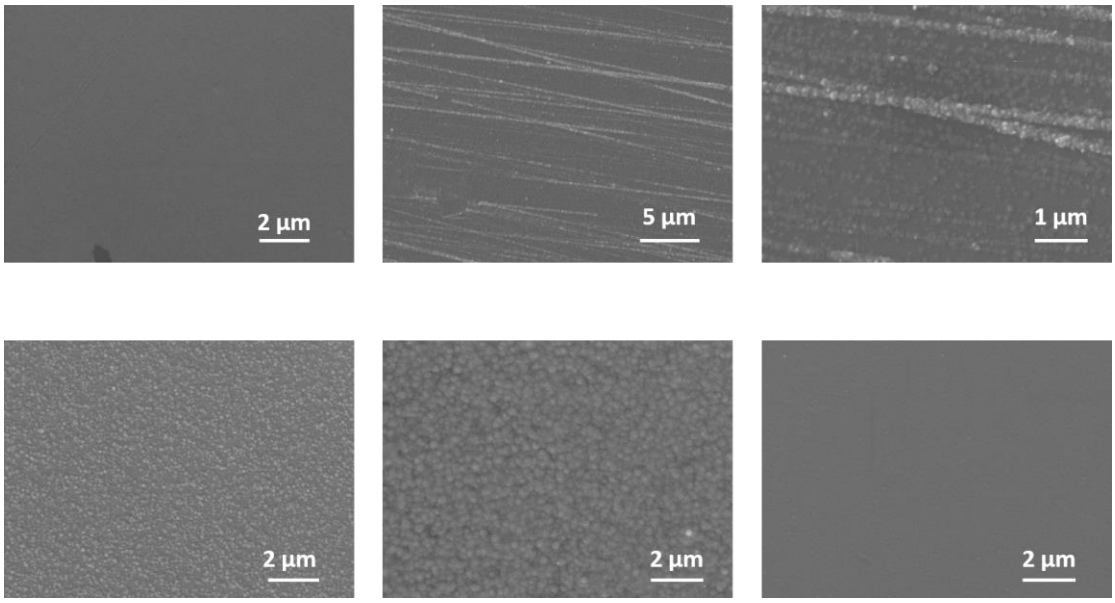


Figure 20. SEM images of (A) Pristine $Cr_2O_3$/Cr/Au/Cr/Si and copper electroplated at 1mA/cm$^2$ for (B)(C) 30 s (D) 1 min on $Cr_2O_3$/Cr/Au/Cr/Si and (E) 5 min (F) 1 min on Au/Cr/Si

The transfer process will depend on the contest between several interfaces. The first one is the interface between electroplated metal and template. Due to the thin layer of $Cr_2O_3$ on ERT ($Cr_2O_3$) template, the Cu is not conformably growing on template like it does for ERT (PFDT) case. Thus, the interaction area between template and

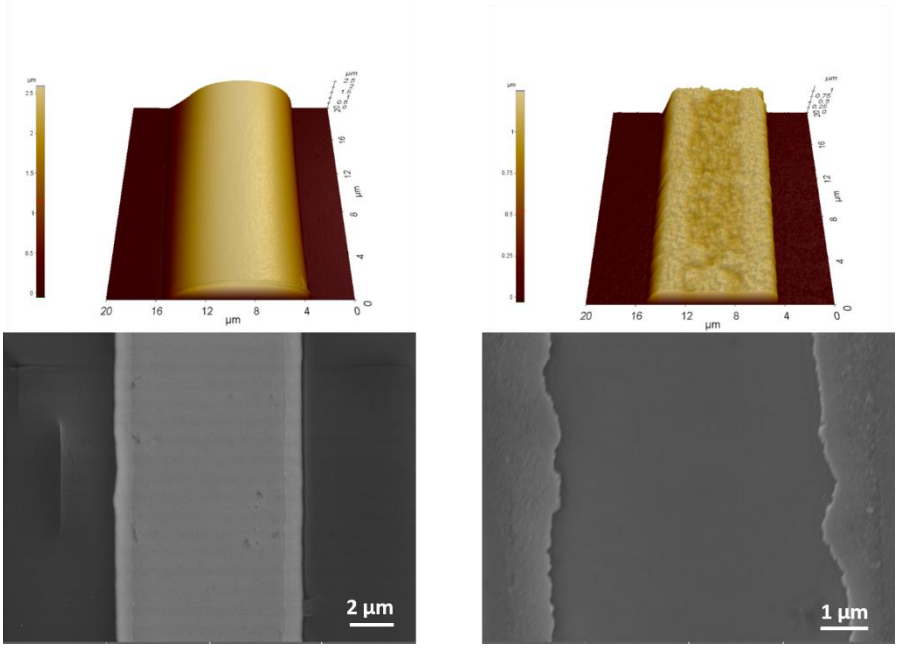


Figure 21. Comparison of morphologies of copper line patterns. (A) AFM image of copper line on template for ERT (PFDT). (B) AFM image of copper line on template for ERT ($Cr_2O_3$). (C) SEM image of copper line made by ERT (PFDT) method after transfer to PET film. (D) SEM image of copper line made by ERT ($Cr_2O_3$) method after transfer to PET film.

electroplated metal is smaller for ERT ($Cr_2O_3$) than ERT (PFDT). And $Cr_2O_3$ has weaker interaction forces with metal compared with the interaction force between Au and metal. This is because when two layers of metals are in close contact, there would be the delocalization of electrons between them which would makes the adhesion between them stronger. From molecular level, $Cr_2O_3$ would have less interaction with plated metal than Au with plated metal. Compared to ERT (PFDT), the surface of electroplated Cu on ERT ($Cr_2O_3$) is rougher and can provide larger surface contact area with adhesives and thus improve the adhesion between adhesive layer and plated metal layer and eases the transfer process.

## 5.4 Conclusion

ERT contains two key steps, electroplating and transfer. The structures of template and electroplating parameters should be considered together and carefully designed to fulfill

the selective electrocrystallization criteria. The successful transfer give credits to the low contact area and low adhesion forces between $Cr_2O_3$/plated metal interface and strong adhesion between adhesive/plated metal interfaces. Both interfaces should be considered for achieving reusable templates.

# Chapter 6: Flexible micro-supercapacitor based on ERT ($Cr_2O_3$) method

## 6.1 Introduction of micro-supercapacitor (MSC)

### 6.1.1 Application of micro-supercapacitor

Miniaturization of electronics are in great need both for military and commercial fields. It has a great impact on the electronics' penetration to society. Recently, improvement of the reliability of wireless communication protocols and emergence of concept "Internet of Things" make the wireless sensor network a great opportunity in various applications. Smart home, health monitor, environment monitor and so on open the market for miniaturized sensors. To realize the autonomy of these sensors, each sensor should have a power supply component for communication and data transfer. And micro-supercapacitor with advantages of cycling stability and higher power density is a promising source to power miniaturized devices. And under some unique scenario, a flexible, bendable and even stretchable miniaturized device is favorable to be physical comfort to use. So flexible micro-supercapacitor as a main component in flexible devices has attracted a lot of attention. In-plane flexible MSC can be easily integrated with other electronic devices which further reduces the place needed and improves the user experience. Researchers have demonstrated the integration of MSC with photodetector[61], gas sensor[62]. For different applications, the electronics have different requirements for power and energy performance.

### 6.1.2 Energy storage mechanism

Electrical charge can be stored in MSC electrode through two charge storage mechanisms, electrical double layer charging and electrochemical charge transfer process.

In electrical double layer charging, charges are stored electrostatically by ion adsorption between the active material and electrolyte interface. Electrochemical charge transfer

process is existed both in battery and capacitor. Conway summarized that three faradaic mechanism that can result in pseudocapacitance, 1) underpotential deposition, 2) redox reaction, and 3) fast intercalation.[63] Underpotential deposition is related to the adsorbed layer between two different metal surfaces. Redox reaction responsible for capacitance usually refers to charge transfer reactions where the current is almost linear to the scan rate. Intercalation capacitance results from ions intercalated into electrode material accompanied by charge transfer with no crystallographic phase change.

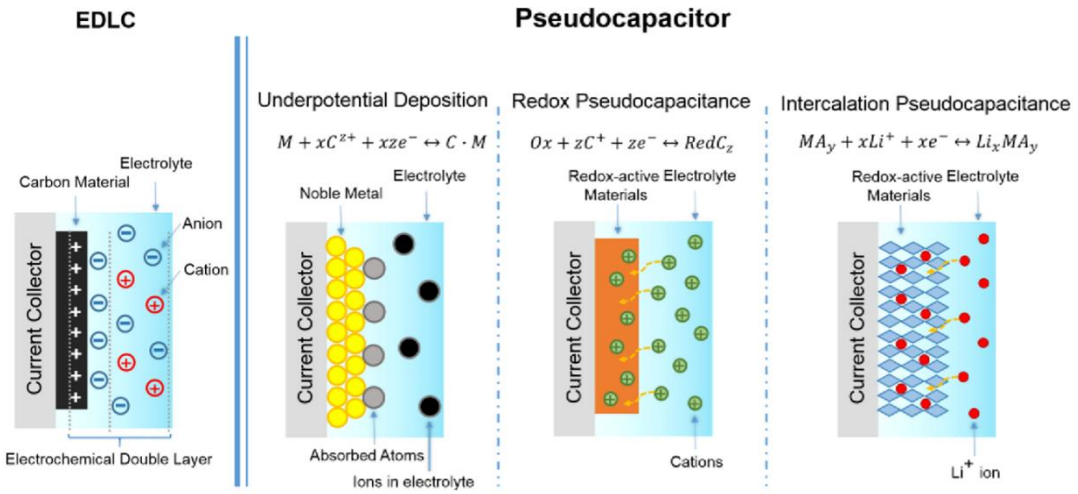


Figure 22. Schematic illustration of charge storage mechanisms of micro-supercapacitor.[64]

Due to the differences in charge storage mechanisms, capacitors charged by electrical double layer can usually provide fast charging/discharging and high stability yet low energy density because it only involves physical adsorption, yet for capacitors charged by faradaic process, they usually have higher energy density but lower stability.

### 6.1.3 Device structures

There are mainly two kinds of architectures for micro-supercapacitors, sandwich structure and in-plane interdigital structure.[65] The first micro-supercapacitor dated back to 2001 is in sandwich configuration with $RuO_2$ as active material and LiPON as separator.[66] One intrinsic problem for capacitor is its low energy density compared with batteries. To improve energy density in sandwich configuration, it is a common way to

increase the thickness of active materials for electrode. However, the resistance of active material increases with the increasing thickness which would also inevitably increases the ion transport resistance and causes poor electrochemical performance such as low power density and low utilization rate. In contrast, micro-supercapacitor with in-plane interdigital structure allows fast ion transport through narrow interspace.[67] By reducing the width of gap ($w_g$), the ion transport resistance can be further decreased which can help improve rate performance.[68] And with multiple open edges, the diffusion of electrolytic ions can be improved even when the active material for electrode is thicker.

And in-plane interdigital mode is more suitable for integration with electronic devices applications in planar structures.[69-72] By optimization of active material, electrolyte and architecture, MSC with both high energy density and power density might be obtained.

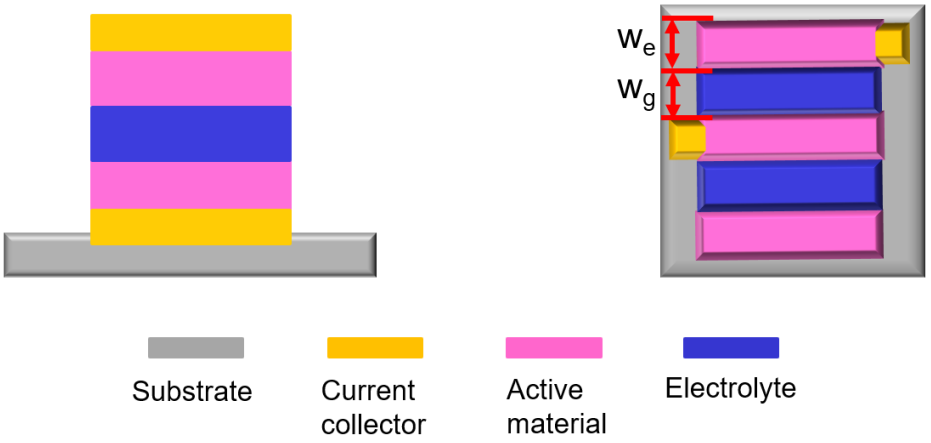


Figure 23. Schematic diagrams of conventional sandwich supercapacitor and micro-supercapacitor with in-plane interdigital electrode architecture.

### 6.1.4 Metrics on electrochemical performance

MSC performance is evaluated by mainly following parameters:

1) Areal capacitance
2) Areal energy density and power density
3) Cycling stability and device lifetime

Considering Helmholtz model for electrical double layer, the amount of charge stored is proportional to applied voltage.

$$C = \frac{Q}{U} = \frac{\varepsilon_0 \varepsilon A}{d}$$

C is capacitance. ε is dielectric constant or relative permittivity of the dielectric medium. Q is the amount of charge stored. U is voltage between two electrode plates. A denotes for electrode/dielectric interface area. And the separation distance between the two electrode plates is denoted as d. $\varepsilon_0$ is vacuum permittivity. The differential form of above equation is shown as below:

$$\frac{dQ}{dt} = C\frac{dU}{dt} + U\frac{dC}{dt} = C\frac{dU}{dt}$$

Considering that current is flow rate of electric charges, it can be written in the following format:

$$i = Cv$$

Above equation shows that the current flowing through a capacitor is independent of voltage applied. So, in cyclic voltammogram (CV), the curve has rectangular shape and

charge and discharge currents are proportional to scan rate. In galvanostatic charge discharge (GCD), a constant current is applied, which indicates the increase rate of voltage is a constant. So, the U-t curve has constant slope. GCD profile is triangular shaped. Through integration of cyclic voltammograms, the amount of charges as a function of potential can be obtained.

$$C = \frac{\Delta Q}{\Delta V} = \frac{\int_0^t i dt}{V}$$

In GCD, the charging discharging current is a constant, so the capacitance can be calculated by:

$$C = \frac{i\Delta t}{\Delta V}$$

We can get power (P) and energy (W) from CV and GCD profile.

$$dW = UdQ = \frac{Q}{C}dQ$$

$$W = \int_0^Q \frac{Q}{C}dQ = \frac{1}{2}\frac{Q^2}{C} = \frac{QU}{C} = \frac{1}{2}CU^2$$

$$P = \frac{W}{t} = \frac{CU^2}{2t}$$

Considering equivalent series resistance, the maximum power output from MSC is:

$$P_{max} = \frac{U^2}{4ESR}$$

We can see from equations above that decreasing equivalent series resistance is favorable for boost electrochemical performance.

Electrochemical impedance spectroscopy can be used to analyze the electrode and electrolyte resistance, charge transfer resistance $R_{ct}$, and ion diffusion. At high frequencies, the capacitance of the electrochemical system can be neglected, so the resistance of this system can be extracted from Nyquist plot. At low frequencies, mass transfer dominates the process, from which Warburg impedance can be obtained. Equivalent series resistance includes the intrinsic resistance of the electrode, the electrolyte resistance and the contact resistance between the current collector and the electrode. Equivalent series resistance is usually determined by the value of real impedance at the frequency of 1 kHz.

In summary, to fabricate MSC with favorable performance, we need to optimize mainly three parameters, the capacitance, working voltage, and equivalent series resistance.

## 6.2 Fabrication of micro-supercapacitor

The fabrication process of micro-supercapacitor is shown in Figure 24. Firstly, the Au current collector was obtained by ERT process. Then, active materials were electrodeposited on the interdigital current collector. Electrolyte was dropped on the surface of interdigital electrodes to obtain micro-supercapacitor devices.

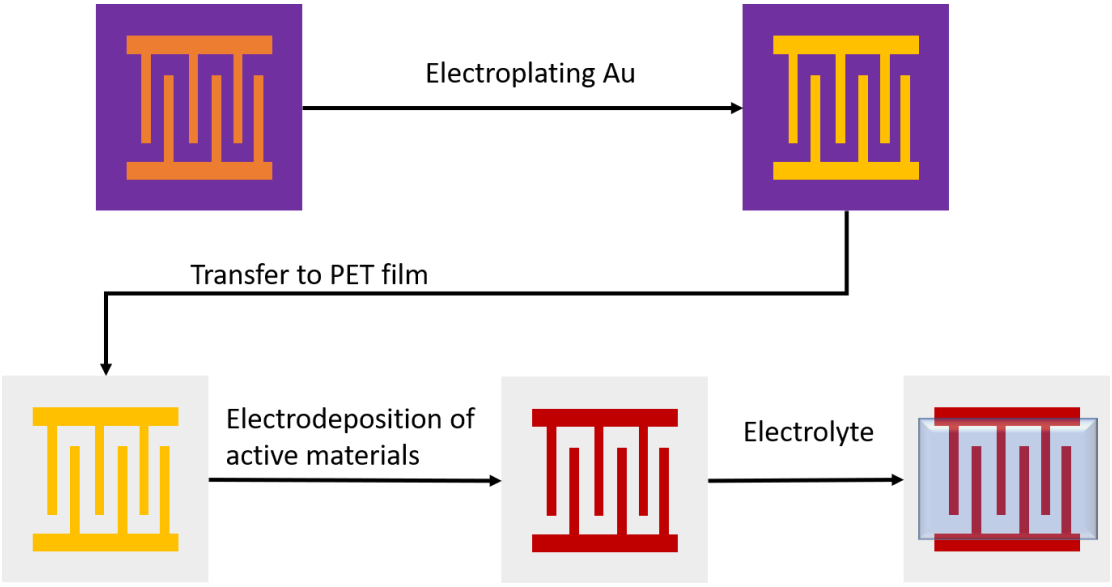

Figure 24. Schematic illustration of fabrication process of micro-supercapacitor.

## 6.3 Characterization of micro-supercapacitor

### 6.3.1 Characterization of electrode

The finger length of gold interdigital electrode is around 1400 μm. The finger width is around 10 μm. The gap between interdigital electrodes is around 5 μm. There are totally 60 pairs of interdigital electrodes. The average thickness of gold electrode is around 0.6 μm. The digital and SEM images of gold electrode and electrode after electroplating $MnO_x$ are shown in Figure 25.

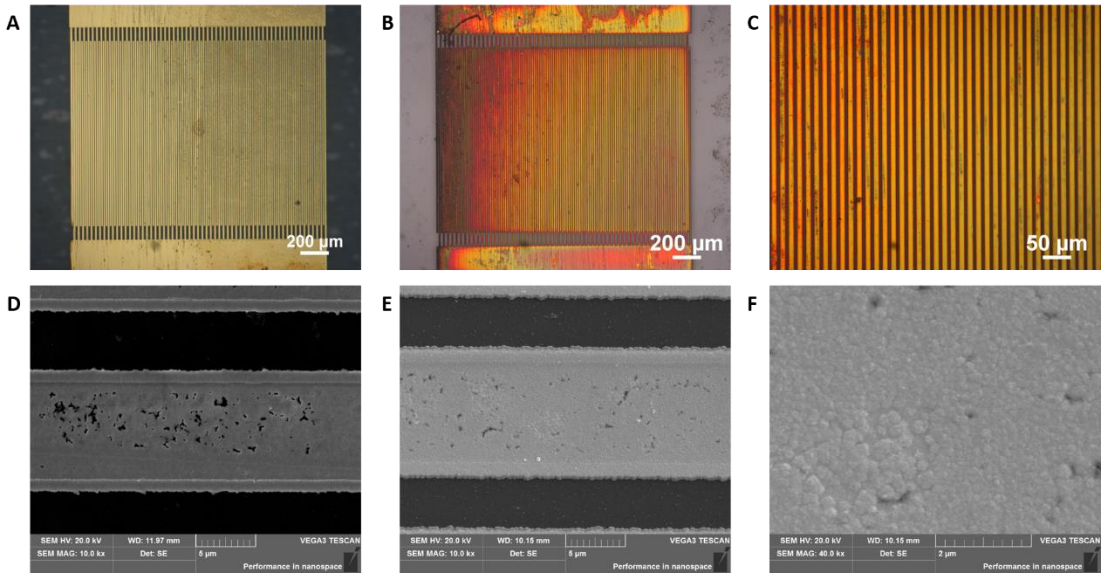


Figure 25. Digital images of (A) Au interdigital current collector, (B) (C) $MnO_x$/Au interdigital electrode, and SEM images of (D) Au current collector, (E) $MnO_x$/Au electrode, (F) $MnO_x$

The phase structure of electroplated gold was obtained using XRD analysis. The sharp peaks can be indexed to the Au (111), (200), (220), and (311) crystal face. The sample was prepared by ERT ($Cr_2O_3$) process with NOA63 as adhesive and PET film as acceptor substrate. The $MnO_x$/Au electrode was characterized with Raman spectroscopy. The broad peaks at $2\theta = 47$ deg and $2\theta = 54$ deg come from the structure of crystalline PET film. Raman shift around 491 $cm^{-1}$ may indicate the deformation mode of Mn-O in $MnO_2$. And the stretching mode of Mn-O in $MnO_6$ octahedra can be shown by the Raman shifts around 562 $cm^{-1}$ and 632 $cm^{-1}$.[73]

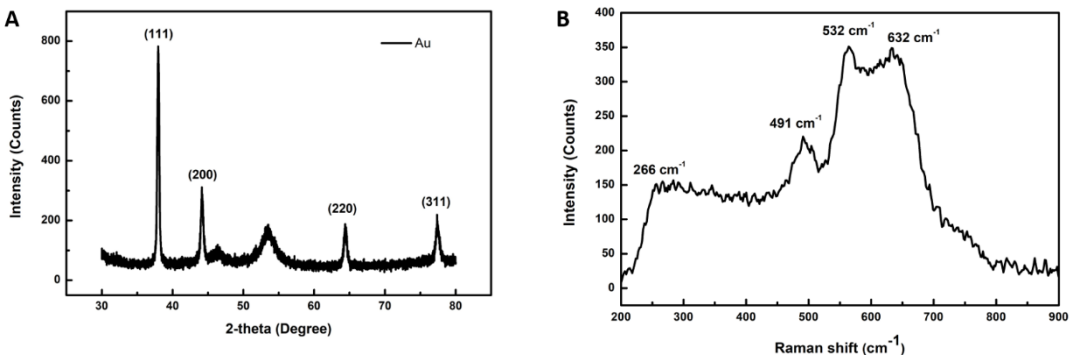


Figure 26. (A) XRD of Au interdigital current collector. (B) Raman spectrum of $MnO_x$ electroplated on Au.

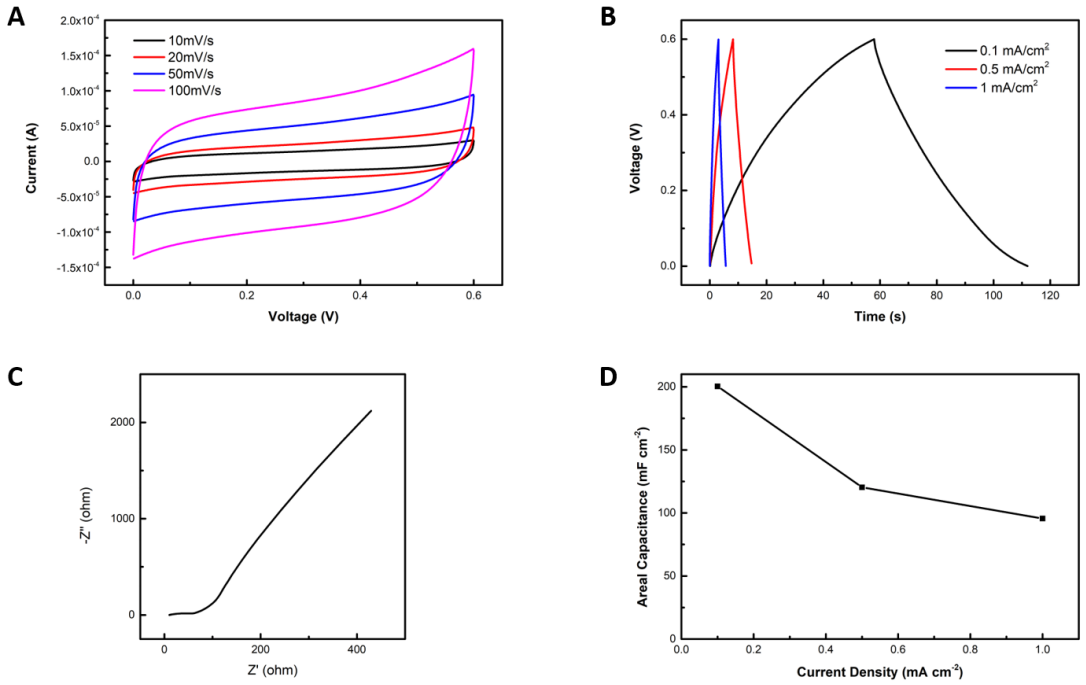


Figure 27. Electrochemical performance of $MnO_x$/Au electrode in 1 M $Na_2SO_4$. (A) CV (B) GCD (C) EIS (D) areal capacitance versus discharge current density

The electrochemical performance of $MnO_x$/Au electrode was tested in 1 M $Na_2SO_4$ under three-electrode configuration with Pt foil as counter electrode and SCE as reference electrode. The areal capacitance was 177 mF $cm^{-2}$ at a discharging current density of 0.1 mA $cm^{-2}$ for electrode with a 60s deposition time for $MnO_x$. The areal capacitance reached 200 mF $cm^{-2}$ for electrode when the deposition time was extended to 90 s for $MnO_x$ at a discharging current density 0.1 mA $cm^{-2}$ The areal capacitance dropped to 185 mF $cm^{-2}$ for electrode 105s deposition time for $MnO_x$. Longer deposition time will cause higher loading amount of $MnO_x$ active material. However, $MnO_x$ is not conductive. Dense $MnO_x$ layer would cause the difficulty in both electron transfer and ion diffusion. The amount of $MnO_x$ should be balanced on account of electron transfer and electrolyte transfer to get the best electrochemical performance. The areal capacitance dropped quickly with the increasing of discharging current density. The areal capacitance dropped to 120 mF $cm^{-2}$ and 95 mF $cm^{-2}$ for discharging current of 0.5 mA $cm^{-2}$ and 1 mA $cm^{-2}$ respectively. This may be caused by insufficient redox reaction under faster charging and discharging process.

The electrochemical impedance spectroscopy were collected using CHI 660e. The applied potential is 0.202 V vs SCE for testing EIS of as obtained $MnO_x$/Au electrode. The frequency ranged from $10^6$ Hz to 0.1 Hz at the amplitude of the sinusoidal voltage of 5 mV. At high frequencies, the capacitance becomes negligible and kinetic of redox reaction dominate the process, so the impedance at high frequencies indicates the resistance of the electrode, which is around 13 Ω for as obtained electrodes in 1 M $Na_2SO_4$ aqueous solution under three electrode configuration. The slope of EIS is nearly vertical at low frequency which indicate a fast and reversible redox process.

### 6.3.2 Electrochemical performance of MSC device

The electrochemical performance of MSC device with 1 M $Na_2SO_4$ as aqueous electrolyte is demonstrated in Figure 28. The $MnO_x$ in the electrodes tested here were obtained by electrodeposition at 15 mA $cm^{-2}$ for 90 s which has the largest areal capacitance in three-electrode configuration test. The areal capacitance of MSC device in 1 M $Na_2SO_4$ is around 1.82 mF $cm^{-2}$ at discharging current of 2 μA. EIS was conducted with initial voltage of 0 V with the frequency ranged from $10^6$ Hz to 0.1 Hz at the amplitude of the sinusoidal voltage of 5 mV. As the figure shows, the impedance of as-obtained microsupercapacitor deviates heavily from ideal semicircle. The shape of EIS depends on the relative values of the kinetic and mass transfer parameters. Since electrochemical process is very complex, it is difficult to analyze EIS with simple equivalent circuits when the EIS curve deviate heavily from curves obtained.

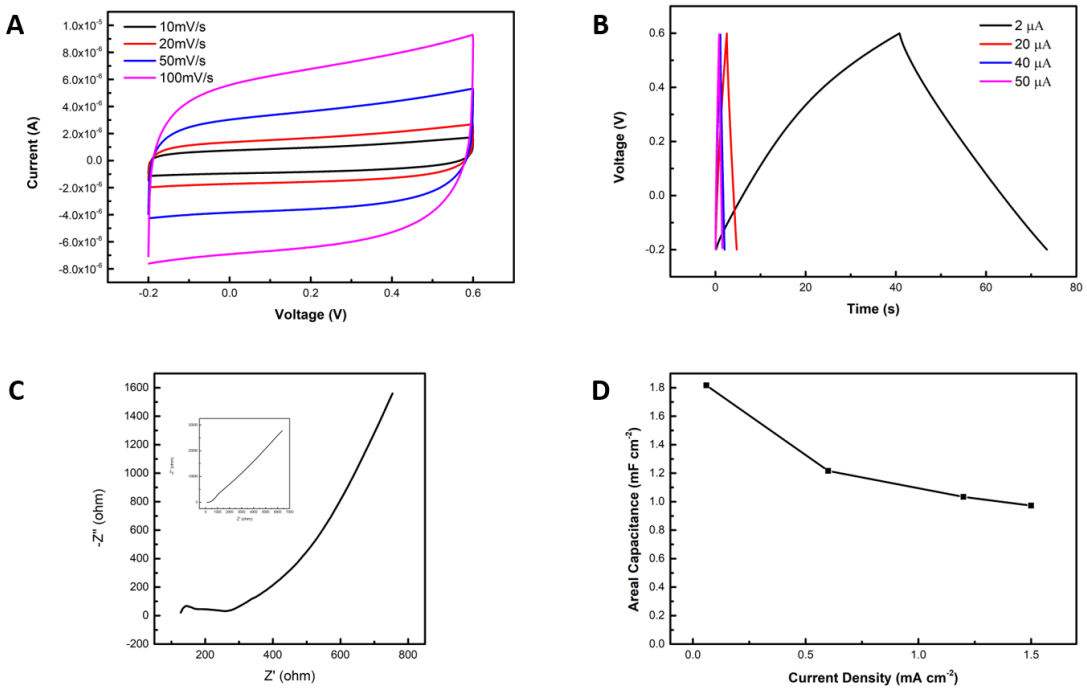


Figure 28. Electrochemical performance of $MnO_x$/Au MSC device with 1 M $Na_2SO_4$ as electrolyte. (A) CV (B) GCD (C) EIS (D) areal capacitance versus discharge current density

The electrochemical performance of MSC device with PVA/LiCl as gel electrolyte was shown in Figure 29. Gel electrolyte is more favorable for fabrication of flexible MSC. Here, commonly used PVA/LiCl electrolyte was dropped on pre-mentioned $MnO_x$/Au electrodes to fabricate MSC devices. MSC devices with different amount of $MnO_x$ were tested with CV, GCD, and EIS. The areal capacitance is calculated with GCD curves for devices with different deposition time of $MnO_x$ at a discharging current of 2 µA. The device with 90 s deposition time shows the best areal capacitance. Therefore, the CV, GCD and EIS of device with 90 s deposition time are shown in the following figure. The areal capacitance of the device reached 2.9 mF $cm^{-2}$. The CV is still rectangular-shaped at large scan rate which may due to by small gap distance between electrodes. The areal capacitance dropped with the increasing of charging and discharging current. The EIS was conducted with initial voltage of -0.03 V with the frequency ranged from $10^6$ Hz to 0.1 Hz at the amplitude of the sinusoidal voltage of 5 mV. From EIS, the electrode resistance was estimated to be 6 Ω for the as-fabricated MSC in PVA/LiCL. The slope of the Nyquist plot in the intermediate frequency region for MSC device in

PVA/LiCl is higher than that for MSC device in $Na_2SO_4$, which indicate a lower Warburg resistance.

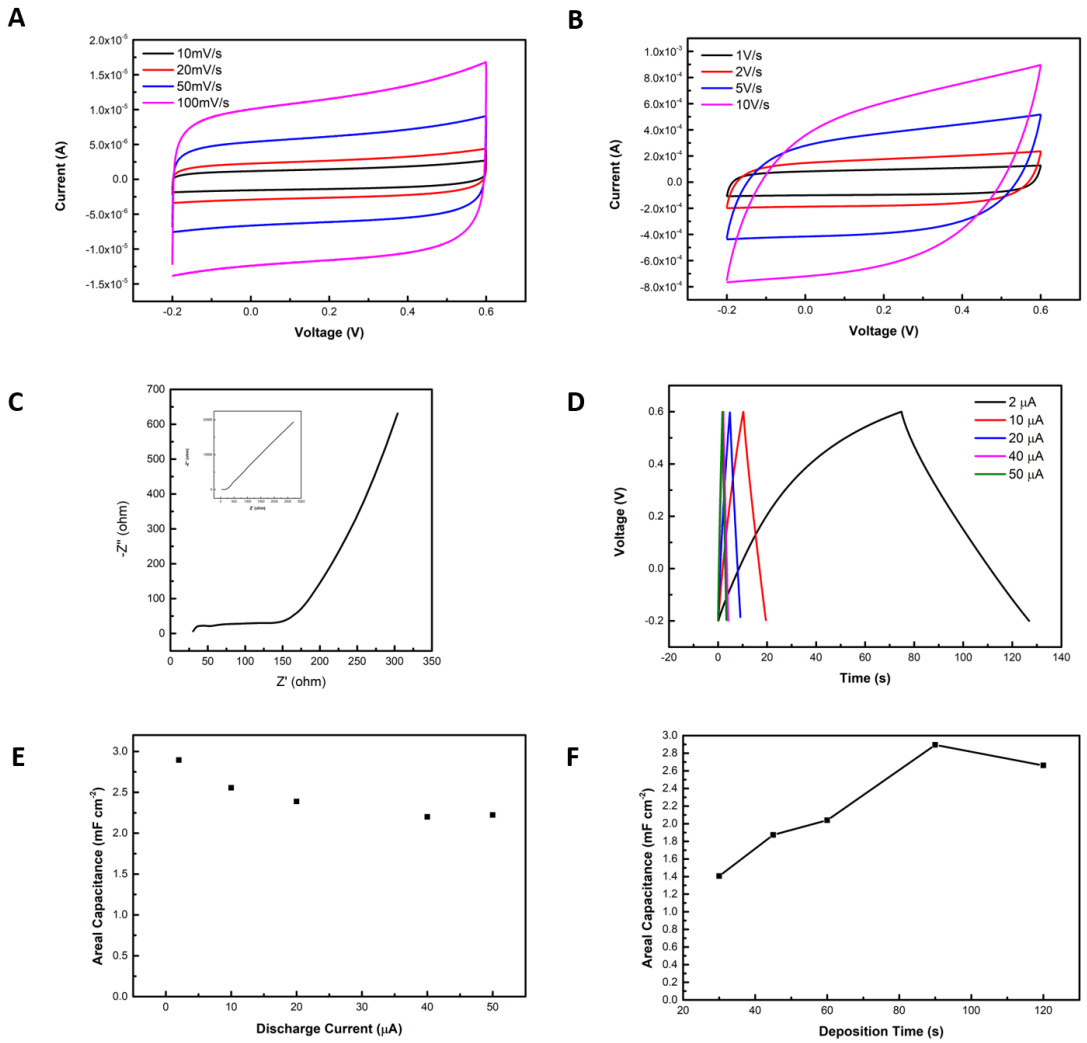


Figure 29. Electrochemical performance of $MnO_x$/Au MSC device with PVA/LiCl as electrolyte. The $MnO_x$ was electrodeposited at 12.5 mA $cm^{-2}$ for 90 s. (A) CV (B) CV at high scan rate (C) EIS (D) GCD (E) areal capacitance versus discharge current density. (F) Areal capacitance versus electrodeposition time

The CV and GCD of MSC under bending were tested to measure the electrochemical stability of devices under bending (Figure 30.). The areal capacitance dropped from 1.23 mF $cm^{-2}$ to 0.93 mF $cm^{-2}$ with the decreasing of bending radius from 8.0 mm to 3.5 mm according to GCD at 2 µA discharging current.

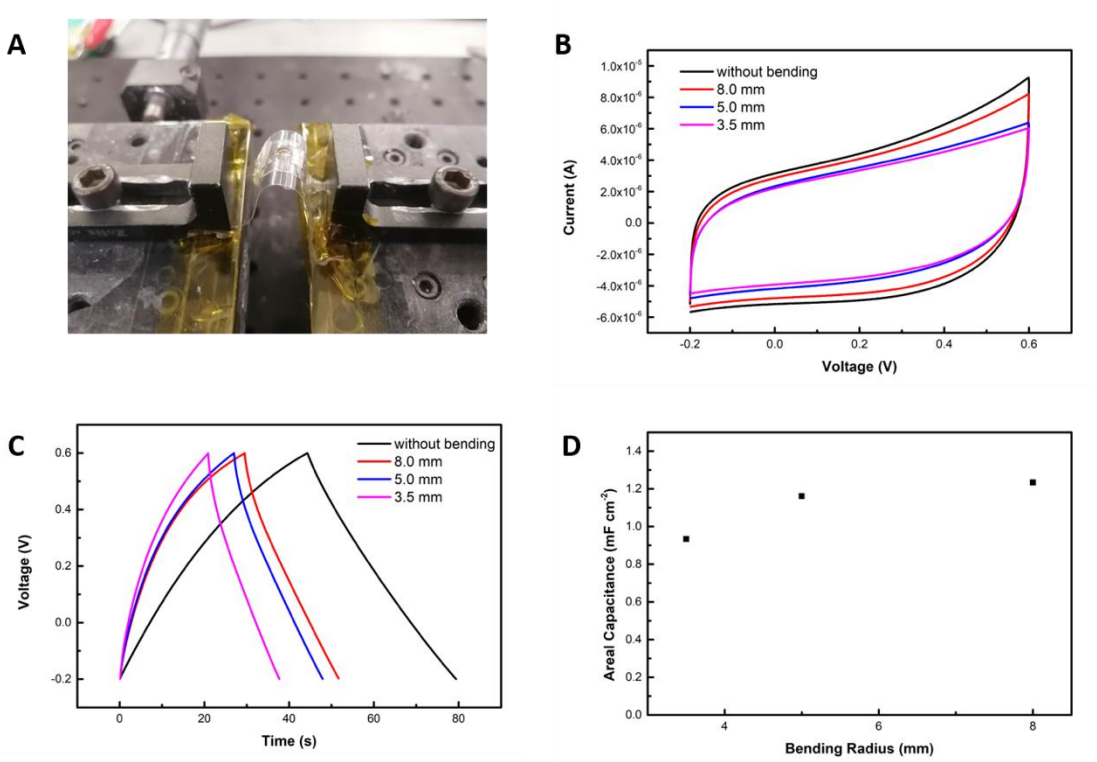


Figure 30. Electrochemical performance of $MnO_x$/Au MSC device with PVA/LiCl as electrolyte under bending. $MnO_x$ was electrodeposited at 12.5 mA $cm^{-2}$ for 60 s. (A) Setup image (B) CV (C) GCD (D) areal capacitance versus bending radius

MSC device with PPy as active material was also fabricated. Electropolymerization of pyrrole on gold interdigital current collectors was conducted with 0.15 M pyrrole and 0.1 M NaTps aqueous solution from -0.7 V to 0.8 V vs SCE at scan rate of 100 mV/s for 2 cycles. More cycles or lower scan rate would cause the interconnection of positive and negative electrodes with PPy and cause short circuit of the device easily. So, the areal capacitance for this device without bending is limited to 0.29 mF $cm^{-2}$ at discharging current of 2 µA which is significantly lower than previously $MnO_x$/Au MSC device. The areal capacitance also suffers from a fast decay during bending which drops from 0.26 mF $cm^{-2}$ under bending radius of 8.0 mm to 0.14 mF $cm^{-2}$ under

bending radius of 3.5 mm. PPy has a better conductivity compared with $MnO_x$. The electrode resistance of PPy is around 2.5 Ω. The equivalent series resistance of PPy/Au MSC device estimated from EIS curve is around 74 Ω which is much lower than that of $MnO_x$/Au MSC device.

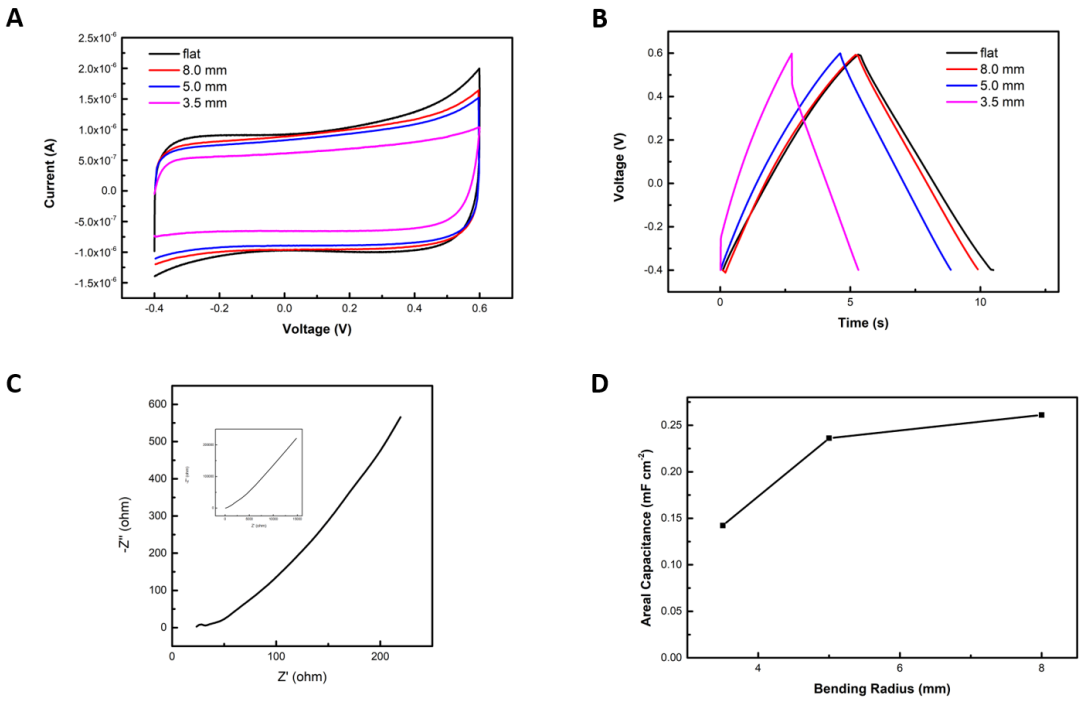


Figure 31. Electrochemical performance of PPy/Au MSC device with PVA/$H_3PO_4$ as electrolyte under bending. (A) CV (B) GCD (C) EIS (D) areal capacitance versus bending radius.

## 6.4 Conclusion

ERT ($Cr_2O_3$) patterning technique was used in the fabrication of high-resolution flexible interdigital electrodes which was later electroplated with active materials to obtain flexible micro-supercapacitor. This shows the application of flexible metal patterns obtained with ERT ($Cr_2O_3$) method in fabrication of MSC device.

# Chapter 7: Conclusions and Suggestions for Future Research

## 7.1 Conclusions

A new release layer is used in electrochemical replication and transfer process. This new release layer ($Cr_2O_3$) shows low adhesion with plated metal film and can be used to fabricate flexible metal patterns and stretchable conductors. The mechanism of ERT with $Cr_2O_3$ were explored. And possible application of flexible metal conductors made by ERT in fabrication of micro-supercapacitor was demonstrated.

In chapter 4, the wide applicability of ERT ($Cr_2O_3$) was demonstrated. It is applicable to fabricate various materials to various geometries of patterns on various substrates. It can be used to fabricate flexible metal patterns and stretchable conductors using different adhesives.

In chapter 5, the mechanism of ERT ($Cr_2O_3$) is studied. ERT includes two essential steps, electroplating and transfer. The difference in conductivity between different regions on the patterned template is the key reason for selective deposition of electroactive materials. The adhesion difference between interfaces is the guiding factor in transfer process. The electroplating process is analyzed from aspects of overpotential, nucleation and growth. The role of $Cr_2O_3$ as release layer is discussed from electrocrystallization aspect. Various structures of template were compared in electroplating process. Due to difference in conductivity and electrocrystallization overpotential, templates with different constructions have different ranges of suitable current density. In transfer process, adhesives were used to transfer the plated metal from donor template to various substrates. Considering the requirements for different applications, photo-curing adhesive and water-soluble tape were used respectively in transfer process to get desired results. The mechanisms for adhesion are discussed to instruct and give explanation for transfer process. The advantages and disadvantages of ERT ($Cr_2O_3$) versus ERT (PFDT) are summarized in detail, which implied different

uses for different release layers.

In chapter 6, the application of ERT ($Cr_2O_3$) in fabrication of micro-supercapacitor was demonstrated. This all solution-processed method is facile and economical for fabrication of micro-supercapacitor. The performance of micro-supercapacitor was evaluated.

In conclusion, $Cr_2O_3$ is developed as a new release layer for electrochemical replication and transfer. The ERT ($Cr_2O_3$) can be used to fabricate patterns of various geometries with various materials on both flexible and stretchable substrates. The mechanism of ERT process is related with structure of template and the role of $Cr_2O_3$ in electrodeposition and transfer. The application of ERT ($Cr_2O_3$) was demonstrated by fabrication of micro-supercapacitor.

## 7.2 Suggestions for future research

ERT with $Cr_2O_3$ can be used to get flexible metal patterns and stretchable conductors. The roughness of the plated metal is not as smooth as ERT with PFDT. One advantage of ERT with $Cr_2O_3$ versus ERT with PFDT is that the adhesion between template and plated metal is lower. Applications that does not require strictly smooth metal patterns can use ERT with $Cr_2O_3$ to fabricate the metal conductor.

The stretchable conductors fabricated by ERT ($Cr_2O_3$) method can be optimized. The structures of stretchable ribbons can be further optimized and the factors that affects obtaining good metal films in electroplating and transfer should be studied in detail. The success rate is currently low and many factors that affect the transfer of metal to PDMS is still not clear. The metal film is prone to fraction and cracks. Better electroplating process and transfer process is needed to make robust metal film.

To further understand the difference in interfaces of ERT ($Cr_2O_3$) method and ERT (PFDT) method, the interface adhesion difference can be studied with theoretical computation.

Although fabrication of micro-supercapacitor has been demonstrated, the performance of micro-supercapacitor is not ideal. Further optimization can be applied to get higher energy density and power density micro-supercapacitor. Gold current collector is of high cost. In the future other metal current collectors should be considered in the fabrication of micro-supercapacitor. Thus, it would become competitive in markets and get its place in the trends of internet of things.

More applications based on ERT ($Cr_2O_3$) can also be studied in the future, for example, transparent heater, organic electrochemical transistors, etc.

# References


1. Richard D. Piner, J. Z., Feng Xu, Seunghun Hong, Chad A. Mirkin, “Dip-Pen” Nanolithography. *Science* **1999,** *283*, 661-663.

2. Mohamed, K., Nanoimprint Lithography for Nanomanufacturing. In *Comprehensive Nanoscience and Nanotechnology*, 2019; pp 357-386.

3. Martinez-Chapa, S. O.; Salazar, A.; Madou, M. J., Two-Photon Polymerization as a Component of Desktop Integrated Manufacturing Platforms. In *Three-Dimensional Microfabrication Using Two-photon Polymerization*, 2016; pp 374-416.

4. Al-Amri, M.; Liao, Z.; Zubairy, M. S., Beyond the Rayleigh Limit in Optical Lithography. In *Advances in Atomic, Molecular, and Optical Physics*, 2012; pp 409-466.

5. Derby, B., Inkjet Printing of Functional and Structural Materials: Fluid Property Requirements, Feature Stability, and Resolution. *Annual Review of Materials Research* **2010,** *40* (1), 395-414.

6. Qin, D.; Xia, Y.; Whitesides, G. M., Soft lithography for micro- and nanoscale patterning. *Nat Protoc* **2010,** *5* (3), 491-502.

7. Cai, S.; Han, Z.; Wang, F.; Zheng, K.; Cao, Y.; Ma, Y.; Feng, X., Review on flexible photonics/electronics integrated devices and fabrication strategy. *Science China Information Sciences* **2018,** *61* (6), 060410.

8. Gates, B. D.; Xu, Q.; Love, J. C.; Wolfe, D. B.; Whitesides, G. M., Unconventional Nanofabrication. *Annual Review of Materials Research* **2004,** *34* (1), 339-372.

9. Wu, W., Inorganic nanomaterials for printed electronics: a review. *Nanoscale* **2017,** *9* (22), 7342-7372.

10. Pimpin, A.; Srituravanich, W., Review on Micro- and Nanolithography Techniques and their Applications. *Engineering Journal* **2012,** *16* (1), 37-56.

11. Khan, S.; Lorenzelli, L.; Dahiya, R. S., Technologies for Printing Sensors and Electronics Over Large Flexible Substrates: A Review. *IEEE Sensors Journal* **2015,** *15*

(6), 3164-3185.

12. Ellmer, K., Past achievements and future challenges in the development of optically transparent electrodes. *Nature Photonics* **2012,** *6* (12), 809-817.

13. Svetlana M. Mitrovski, S. A., Evan M. Erickson,; Matthew E. Stewart, J. A. R., and Ralph G. Nuzzo, Soft Lithography for Microfluidic Microelectromechanical Systems (MEMS) and Optical Devices. *Hoboken, N.J. :: Wiley* **2008**, pp. 293 - 323.

14. Geissler, M.; Xia, Y., Patterning: Principles and Some New Developments. *Advanced Materials* **2004,** *16* (15), 1249-1269.

15. Bhure, R.; Mahapatro, A., Surface Patterning Using Self Assembled Monolayers (SAMs). In *Biomaterials*, American Chemical Society: 2010; Vol. 1054, pp 65-107.

16. Harvey, E.; Ghantasala, M., Nanofabrication. In *Nanostructure Control of Materials*, 2006; pp 303-330.

17. Takashi Ito, S. O., Pushing the limits of lithography. *Nature* **2000,** *406*, 1027-1031.

18. Okazaki, S., High resolution optical lithography or high throughput electron beam lithography: The technical struggle from the micro to the nano-fabrication evolution. *Microelectronic Engineering* **2015,** *133*, 23-35.

19. Rothschild, M., Projection optical lithography. *Materials Today* **2005,** *8* (2), 18-24.

20. Ryusho Hirose, I.-c., Nakahara -ku, Kawasaki -shi, Kanagawa -ken, New g-line Lens for Next Generation. *Proc. SPIE* **1989,** *1088*, 178-186.

21. H. L. Stover, M. N., I. Bol, V. Miller, Submicron optical lithography: I-line lens and photoresist technology. *Proc. SPIE* **1984,** *470*, 22-33.

22. Jian K., W. C. G., Lin B. J. , Ultrafast High-Resolution Contact Lithography with Excimer Lasers. *J. Res. Develop.* **1982,** *26* (2), 151-159.

23. Nomura. N. , N. H., Tani Y., Koga K. , Araki* N., Satot T., Sasago M., ArF quarter-micron projection lithography with an aspherical lens system *Microelectronic Engineering* **1990,** *11*, 183-186.

24. Bloomstein, T. M., Lithography with 157 nm lasers. *Journal of Vacuum Science & Technology B: Microelectronics and Nanometer Structures* **1997,** *15* (6).

25. Gwyn, C. W., Extreme ultraviolet lithography. *Journal of Vacuum Science & Technology B: Microelectronics and Nanometer Structures* **1998,** *16* (6).

26. Williamson, D. M., DUV or EUV, that is the question. *Proc. SPIE* **2000,** *4146*, 1-12.

27. Switkes, M.; Rothschild, M., Immersion lithography at 157 nm. *Journal of Vacuum Science & Technology B: Microelectronics and Nanometer Structures* **2001,** *19* (6).

28. Li, L.; Liu, X.; Pal, S.; Wang, S.; Ober, C. K.; Giannelis, E. P., Extreme ultraviolet resist materials for sub-7 nm patterning. *Chem Soc Rev* **2017,** *46* (16), 4855-4866.

29. Reichmanis E. , H. F. M., Nalamasu O., Neenan T. X. , Chemically Amplified Resists: Chemistry and Processes. *ADVANCED MATERIALS FOR OPTICS AND ELECTRONICS* **1994,** *4*, 83-93.

30. Yuko Kaimoto, K. N., Satoshi Takechi, and Naomichi Abe, Alicyclic Polymer for ArF and KrF Excimer Resist Based on Chemical Amplification. *Proc. SPIE* **1992,** *1672*, 67-73.

31. Kwak, M. K.; Guo, L. J., Phase-Shift Lithography. In *Encyclopedia of Microfluidics and Nanofluidics*, 2014; pp 1-10.

32. Miyoko Noguchi, M. M., Yuuichi Iwasaki and Akiyoshi Suzuki, Subhalf Micron Lithography System with Phase- Shifting Effect. *Proc. SPIE 1674*, 92-104.

33. John P. Stirniman, M. L. R., Fast proximity correction with zone sampling. *Proc. SPIE* **1994,** *2197*, 294-301.

34. Alan E. Rosenbiuth, S. B., Michael Hibbs, Kafai Lai, Antoinette Molless, Rama N. Singh, Alfred wong, Optimum Mask and Source Patterns to Print a Given Shape. *Proc. SPIE* **2001,** *4346*, 486-502.

35. Chen, Y., Nanofabrication by electron beam lithography and its applications: A review. *Microelectronic Engineering* **2015,** *135*, 57-72.

36. Li, K.; Li, J.; Reardon, C.; Schuster, C. S.; Wang, Y.; Triggs, G. J.; Damnik, N.; Muenchenberger, J.; Wang, X.; Martins, E. R.; Krauss, T. F., High speed e-beam writing for large area photonic nanostructures - a choice of parameters. *Sci Rep* **2016,** *6*, 32945.

37. Greve, M. M.; Holst, B., Optimization of an electron beam lithography instrument for fast, large area writing at 10 kV acceleration voltage. *Journal of Vacuum Science & Technology B, Nanotechnology and Microelectronics: Materials, Processing, Measurement, and Phenomena* **2013,** *31* (4).

38. Stephen Y. Chou, P. R. K., Preston J. Renstrom, Imprint Lithography with 25-Nanometer Resolution. *Science* **1996,** *272*, 85-87.

39. Traub, M. C.; Longsine, W.; Truskett, V. N., Advances in Nanoimprint Lithography. *Annual Review of Chemical and Biomolecular Engineering* **2016,** *7* (1), 583-604.

40. Paolo Lugli, S. M., IEEE, Stefan Harrer, Sebastian Strobel, Francesca Brunetti, Giuseppe Scarpa, Marc Tornow, Gerhard Abstreiter, Advances in Nanoimprint Lithography. *Proceedings of the 7th IEEE International Conference on Nanotechnology* **2007**.

41. Younan Xia, G. M. W., Soft Lithography. *Angew. Chem. Int. Ed* **1998,** *37*, 550-575.

42. Younan Xia, G. M. W., SOFT LITHOGRAPHY. *Annu. Rev. Mater. Sci.* **1998,** *28*, 153-184.

43. Amit Kumar, G. M. W., Features of gold having micrometer to centimeter dimensions can be formed through a combination of stamping with an elastomeric stamp and an alkanethiol "ink" followed by chemical etching. *Appl. Phys. Lett* **1993,** *63* (14).

44. Kumar, A.; Biebuyck, H. A.; Whitesides, G. M., Patterning Self-Assembled Monolayers: Applications in Materials Science. *Langmuir* **1994,** *10* (5), 1498-1511.

45. Gates, B. D.; Xu, Q.; Stewart, M.; Ryan, D.; Willson, C. G.; Whitesides, G. M., New Approaches to Nanofabrication: Molding, Printing, and Other Techniques. *Chemical Reviews* **2005,** *105* (4), 1171-1196.

46. Lee, J. N.; Park, C.; Whitesides, G. M., Solvent Compatibility of Poly(dimethylsiloxane)-Based Microfluidic Devices. *Analytical Chemistry* **2003,** *75* (23), 6544-6554.

47. Emmanuel Delamarche, H. S., Bruno Michel. and Hans Biebuyck, Stability of Molded Polydimethylsiloxane Microstructures. *Adv. Mater.* **1997,** *9*, 741-746.

48. Tseng, A. A.; Notargiacomo, A.; Chen, T. P., Nanofabrication by scanning probe microscope lithography: A review. *Journal of Vacuum Science & Technology B: Microelectronics and Nanometer Structures* **2005,** *23* (3).

49. Liu, G.; Petrosko, S. H.; Zheng, Z.; Mirkin, C. A., Evolution of Dip-Pen Nanolithography (DPN): From Molecular Patterning to Materials Discovery. *Chem Rev* **2020,** *120* (13), 6009-6047.

50. D. M. Eigler, E. K. S., Positioning single atoms with a scanning tunnelling microscope. *Nature* **1990,** *344*, 524-526.

51. Terris, B. D.; Mamin, H. J.; Best, M. E.; Logan, J. A.; Rugar, D.; Rishton, S. A., Nanoscale replication for scanning probe data storage. *Applied Physics Letters* **1996,** *69* (27), 4262-4264.

52. Heiko Wolf, Y. K. R. C., Seigfried Karg, Phillip Mensch, Christian Schewemmer, Armin Knoll, Thermal scanning probe lithography for nano-fabrication. *Proceedings of the SMTA Pan Pacific Microelectronics Symposium 2019* **2019**.

53. Shim, W.; Braunschweig, A. B.; Liao, X.; Chai, J.; Lim, J. K.; Zheng, G.; Mirkin, C. A., Hard-tip, soft-spring lithography. *Nature* **2011,** *469* (7331), 516-20.

54. Moonen, P. F.; Yakimets, I.; Huskens, J., Fabrication of transistors on flexible substrates: from mass-printing to high-resolution alternative lithography strategies. *Advanced Materials* **2012,** *24* (41), 5526-41.

55. Nayak, L.; Mohanty, S.; Nayak, S. K.; Ramadoss, A., A review on inkjet printing of nanoparticle inks for flexible electronics. *Journal of Materials Chemistry C* **2019,** *7* (29), 8771-8795.

56. Liu, Y.; Derby, B., Experimental study of the parameters for stable drop-on-demand inkjet performance. *Physics of Fluids* **2019,** *31* (3).

57. Martin, G. D.; Hoath, S. D.; Hutchings, I. M., Inkjet printing - the physics of manipulating liquid jets and drops. *Journal of Physics: Conference Series* **2008,** *105*.

58. Matsuhisa, N.; Chen, X.; Bao, Z.; Someya, T., Materials and structural designs of stretchable conductors. *Chem Soc Rev* **2019,** *48* (11), 2946-2966.

59. Nguyen, T.; Khine, M., Advances in Materials for Soft Stretchable Conductors and Their Behavior under Mechanical Deformation. *Polymers (Basel)* **2020,** *12* (7).

60. Park, M.; Im, J.; Shin, M.; Min, Y.; Park, J.; Cho, H.; Park, S.; Shim, M. B.; Jeon, S.; Chung, D. Y.; Bae, J.; Park, J.; Jeong, U.; Kim, K., Highly stretchable electric circuits from a composite material of silver nanoparticles and elastomeric fibres. *Nat Nanotechnol* **2012,** *7* (12), 803-9.

61. Gu, S. S.; Lou, Z.; Li, L. D.; Chen, Z. J.; Ma, X. D.; Shen, G. Z., Fabrication of flexible reduced graphene oxide/Fe2O3 hollow nanospheres based on-chip micro-supercapacitors for integrated photodetecting applications. *Nano Res.* **2016,** *9* (2), 424-434.

62. Yun, J.; Lim, Y.; Jang, G. N.; Kim, D.; Lee, S.-J.; Park, H.; Hong, S. Y.; Lee, G.; Zi, G.; Ha, J. S., Stretchable patterned graphene gas sensor driven by integrated micro-supercapacitor array. *Nano Energy* **2016,** *19*, 401-414.

63. Conway, B. E., *Electrochemical Supercapacitors: Scientific Fundamentals and Technological Applications*. KluwerAcademic: 1999.

64. Augustyn, V.; Simon, P.; Dunn, B., Pseudocapacitive oxide materials for high-rate electrochemical energy storage. *Energy & Environmental Science* **2014,** *7* (5).

65. Guo, R. S.; Chen, J. T.; Yang, B. J.; Liu, L. Y.; Su, L. J.; Shen, B. S.; Yan, X. B., In-Plane Micro-Supercapacitors for an Integrated Device on One Piece of Paper. *Adv. Funct. Mater.* **2017,** *27* (43), 11.

66. Jae Hong Lim, D. J. C., Han-Ki Kim, Won Il Cho, and Young Soo Yoon, Thin Film Supercapacitors Using a Sputtered RuO2 Electrode. *J. Power Sources* **2001,** *148* (3), 4.

67. Niu, Z. Q.; Zhang, L.; Liu, L.; Zhu, B. W.; Dong, H. B.; Chen, X. D., All-Solid-State Flexible Ultrathin Micro-Supercapacitors Based on Graphene. *Adv. Mater.* **2013,**

*25* (29), 4035-4042.

68. Dinh, T. M.; Armstrong, K.; Guay, D.; Pech, D., High-resolution on-chip supercapacitors with ultra-high scan rate ability. *J. Mater. Chem. A* **2014,** *2* (20), 7170-7174.

69. Wu, Z. S.; Parvez, K.; Feng, X. L.; Mullen, K., Graphene-based in-plane micro-supercapacitors with high power and energy densities. *Nat. Commun.* **2013,** *4*, 8.

70. Xu, J.; Shen, G. Z., A flexible integrated photodetector system driven by on-chip microsupercapacitors. *Nano Energy* **2015,** *13*, 131-139.

71. Cai, J. G.; Lv, C.; Watanabe, A., Laser direct writing of high-performance flexible all-solid-state carbon micro-supercapacitors for an on-chip self-powered photodetection system. *Nano Energy* **2016,** *30*, 790-800.

72. Zhang, X. Y.; Zhao, W.; Wei, L.; Jin, Y. Y.; Hou, J.; Wang, X. X.; Guo, X., In-plane flexible solid-state microsupercapacitors for on-chip electronics. *Energy* **2019,** *170*, 338-348.

73. Barai, H. R.; Banerjee, A. N.; Hamnabard, N.; Joo, S. W., Synthesis of amorphous manganese oxide nanoparticles – to – crystalline nanorods through a simple wet-chemical technique using K+ ions as a ‘growth director’ and their morphology-controlled high performance supercapacitor applications. *RSC Advances* **2016,** *6* (82), 78887-78908.